ESTCP
Cost and Performance Report

(ER-201118)

Demonstration of a Fractured Rock Geophysical Toolbox for Characterization and Monitoring of DNAPL Biodegradation in Fractured Rock Aquifers

September 2015

This document has been cleared for public release; Distribution Statement A

ESTCP

ENVIRONMENTAL SECURITY
TECHNOLOGY CERTIFICATION PROGRAM

U.S. Department of Defense

REPORT DOCUMENTATION PAGE

Form Approved
OMB No. 0704-0188

The public reporting burden for this collection of information is estimated to average 1 hour per response, including the time for reviewing instructions, searching existing data sources, gathering and maintaining the data needed, and completing and reviewing the collection of information. Send comments regarding this burden estimate or any other aspect of this collection of information, including suggestions for reducing the burden, to Department of Defense, Washington Headquarters Services, Directorate for Information Operations and Reports (0704-0188), 1215 Jefferson Davis Highway, Suite 1204, Arlington, VA 22202-4302. Respondents should be aware that notwithstanding any other provision of law, no person shall be subject to any penalty for failing to comply with a collection of information if it does not display a currently valid OMB control number.
PLEASE DO NOT RETURN YOUR FORM TO THE ABOVE ADDRESS.

1. REPORT DATE *(DD-MM-YYYY)*
25-09-2015

2. REPORT TYPE
Cost and Performance Report

3. DATES COVERED *(From - To)*
June 2011 to June 2015

4. TITLE AND SUBTITLE
Demonstration of a Fractured Rock Geophysical Toolbox (FRGT) for Characterization and Monitoring of DNAPL Biodegradation in Fractured Rock Aquifers

5a. CONTRACT NUMBER
W912HQ-11-C-0027

5b. GRANT NUMBER

5c. PROGRAM ELEMENT NUMBER

6. AUTHOR(S)
L. Slater, F. Day-Lewis, J. Robinson and T. Johnson

5d. PROJECT NUMBER
ER-201118

5e. TASK NUMBER

5f. WORK UNIT NUMBER

7. PERFORMING ORGANIZATION NAME(S) AND ADDRESS(ES)
Rutgers University-Newark
Department of Earth/Environmental Science
101 Warren Street
Newark, NJ 07102

8. PERFORMING ORGANIZATION REPORT NUMBER
DEES-1

9. SPONSORING/MONITORING AGENCY NAME(S) AND ADDRESS(ES)
Environmental Security and Technology Certification Program
4800 Mark Center Drive, Suite 17D08
Alexandria, VA 22350

10. SPONSOR/MONITOR'S ACRONYM(S)
ESTCP

11. SPONSOR/MONITOR'S REPORT NUMBER(S)
ER-201118

12. DISTRIBUTION/AVAILABILITY STATEMENT
Approved for public release; distribution is unlimited

13. SUPPLEMENTARY NOTES

14. ABSTRACT

Contaminated sites in fractured rock are particularly difficult and expensive to remediate, because characterization and monitoring is problematic in the presence of extreme heterogeneity. The performance objectives of this demonstration focused on evaluating: [1] fracture network characterization using a fractured rock geophysics toolbox (FRGT); [2] autonomous monitoring of amendment delivery and subsequent contaminant biodegradation using geophysical technologies that sense beyond the borehole; [3] application of an 'informed inversion strategy' to improve the geophysical imaging of fractured rock settings relative to what can currently be achieved with off-the-shelf functionality. Specific performance objectives were largely met, although the physical characteristics of the primary demonstration site, being the Naval Air Warfare Center (NAWC) in W. Trenton (NJ), limited the performance of some methods in the FRGT.

15. SUBJECT TERMS
Fractured rock, Electrical geophysics, amendment monitoring

16. SECURITY CLASSIFICATION OF:			17. LIMITATION OF ABSTRACT	18. NUMBER OF PAGES	19a. NAME OF RESPONSIBLE PERSON
a. REPORT	b. ABSTRACT	c. THIS PAGE			Lee Slater
U	U	U	UU	44	19b. TELEPHONE NUMBER *(Include area code)* 973-353-5109

Reset

Standard Form 298 (Rev. 8/98)
Prescribed by ANSI Std. Z39.18

COST & PERFORMANCE REPORT
Project: ER-201118

TABLE OF CONTENTS

		Page
EXECUTIVE SUMMARY		ES-1
1.0	INTRODUCTION	1
1.1	BACKGROUND	1
1.2	OBJECTIVES OF THE DEMONSTRATION	1
1.3	REGULATORY DRIVERS	1
2.0	TECHNOLOGY	3
2.1	TECHNOLOGY DESCRIPTION	3
2.2	ADVANTAGES AND LIMITATIONS OF THE TECHNOLOGY	4
3.0	PERFORMANCE OBJECTIVES	5
4.0	SITE DESCRIPTION	9
4.1	SITE LOCATION	9
4.2	SITE GEOLOGY/HYDROGEOLOGY	9
10		
5.0	TEST DESIGN	13
5.1	CONCEPTUAL EXPERIMENTAL DESIGN	13
5.2	BASELINE CHARACTERIZATION	13
5.2.1	Drilling, Coring, and Well Installation	13
5.2.2	Geophysical Logging	15
5.2.3	Hydraulic Testing	15
5.3	LABORATORY STUDY RESULTS	16
5.3.1	Amendment Selection Process	16
5.4	FIELD TESTING	17
5.4.1	Static ERT Characterization	17
5.5	SAMPLING METHODS	18
5.5.1	ERT Tracer tests and Amendment Injections	18
5.5.1.1	Overview	18
5.5.1.2	87BR-85BR	18
5.5.1.3	ERT Monitoring of Amendment Injection into 87BR	20
5.6	SAMPLING RESULTS	20
5.6.1	87BR-85BR	20
5.6.2	Amendment Injection	24
6.0	PERFORMANCE ASSESSMENT	28
6.1	ASSESSMENT OF CHARACTERIZATION IMAGING AT NAWC	28
6.2	ASSESSMENT OF TRACER TESTS	29
6.2.1	87BR-85BR	30
6.2.2	Amendment Injection	32

TABLE OF CONTENTS (continued)

Page

7.0 COST ASSESSMENT 36
- 7.1 COST MODEL 36
- 7.2 COST DRIVERS 37
- 7.3 COST ANALYSIS 37

8.0 IMPLEMENTATION ISSUES 41
- 8.1 REGULATORY ISSUES 41
- 8.2 END-USER CONCERNS 41
- 8.3 PROCUREMENT ISSUES 41

9.0 REFERENCES 44

APPENDIX A POINTS OF CONTACT A-1

LIST OF FIGURES

Page

Figure 1. Summary schematic of the FRGT technology. 3
Figure 2. NAWC site location. 8
Figure 3. Section F-F (see Figure 2) showing geologic cross section in the vicinity of 83-89BR boreholes. 9
Figure 4. Peak molar concentrations of original TCE at wells in the vicinity of 83-89BR for samples collected between 1990-2014. 9
Figure 5. Cross section F-F' showing the selected region bounded by the array of boreholes selected for this demonstration. 10
Figure 6. As-built borehole schematic. 12
Figure 7. Drill rig and site view (a), and aerial photo showing drilling locations (b). 13
Figure 8. Borehole section view for 83-89BR wells. 13
Figure 9. Hydraulic interpretation from drawdown data alongside caliper and ATV borehole logs. 15
Figure 10. Electrical resistivity image for slice 85-83-87 with fracture intersection depths and packers, and strike-dip 3D orientation. 16
Figure 11. Field set-up for 87BR-85BR tracer test during extraction from 85BR. 17
Figure 12. Flow chart of tracer test where numbers of ERT data acquisitions and water samples are indicated in parentheses ( ). 18
Figure 13. A subset of vertical apparent conductivity depth profiles for wells showing the largest conductivity changes: 87BR, 83BR, 85BR before and during the four-part tracer test. 20
Figure 14. Time-lapse ERT image of relative change in electrical conductivity (condt = conductivity at time slice 't', cond0 = conductivity of background) during tracer injection showing (A) plan view (B) elevation view. 22
Figure 15. Time-lapse ERT images of relative change in electrical conductivity (Condt = conductivity at time slice 't', Cond0 = conductivity of background) following the conductive tracer injection. 23
Figure 16. Vertical ERT profiles within injection borehole 87BR and boreholes with the largest conductivity changes, 83BR and 85BR. 25
Figure 17. Elevation view of time-lapse 3D ERT conductivity changes during and post amendment injection. 26
Figure 18. Plan view of time-lapse 3D ERT conductivity changes during and post amendment injection. 27
Figure 19. Electrical resistivity image for slice 85-83-87 with fracture intersection depths, packers and strike/dip of formation noted, showing alternating conductive and resistive layering partly resulting from the alternating laminated and massive mudstones at the site. 28
Figure 20. Interpretation of hydraulically connected pathways from cross-borehole drawdown data. 29
Figure 21. Fluid specific conductance and bromide concentrations for samples from 85BR during the 87BR-85BR ERT tracer injection test. 30

LIST OF FIGURES (continued)

Page

Figure 22. Bromide and changes in fluid specific conductance (SC) show similar trends in the 87-85BR tracer test (R2=0.67) (a) and sulfate concentrations and changes in SC show a significant correlation in the 87-85BR tracer test (R2=0.72) (b). 31

Figure 23. A visual comparison of absolute changes in a) TCE; b) DCE; c) VC concentrations prior to and after the amendment injection within sampled boreholes 83BR, 84BR, 85BR and 87BR; and d) Percent changes in concentrations from initial values (7/9/2014) of TCE, DCE, and VC within 83BR, 84BR, 85BR and 87BR. 33

Figure 24. (a) Hypothetical amendment-treated fracture zone including surface area calculation, (b) estimated amendment-treated fracture zone based on ERT between 7 boreholes, and (c) estimated amendment-treated fracture zone inferred from direct sampling at 16 wells on a regular grid. 39

Figure 25. Estimated surface area for direct sampling on a regular grid, compared to ERT-estimated surface area for 7 wells, and true surface area. 40

LIST OF TABLES

Page

Table 1. Summary of primary performance objectives, associated data requirements and success criteria as defined in the demonstration plan performance objective. 5
Table 2. Borehole logging methods used in 83BR-89BR. 144
Table 3. ERT tracer test details for 87BR-85BR. 188
Table 4. Water sample analysis of key compounds in boreholes 83BR, 84BR, 85BR, and 87BR prior to and after amendment injection in 87BR. 32
Table 5. Cost model for implementation of time-lapse 3D electrical tomography at the NAWC site. 366
Table 6. Cost model for implementation of time-lapse 3D electrical tomography under scenario 2. 388

This page was left blank intentionally.

ACRONYMS AND ABBREVIATIONS

3D	three dimensional
ANOVA	analysis of variance
ATV	acoustical televiewer
BHGPR	borehole ground penetrating radar
bls	below land surface
cDCE	cis-dichloroethylene
COTS	commercial off-the-shelf
CVOC	chlorinated volatile organic compound
DBHGPR	directional cross borehole ground penetrating radar
DI	deionized water
DNAPL	dense non-aqueous phase liquid
DoD	U.S. Department of Defense
E4D	4D electrical resistivity tomography forward and inverse modeling code
EPA	U.S. Environmental Protection Agency
ERI	electrical resistivity imaging
ERT	electrical resistivity tomography
FRGT	fractured rock geophysical toolbox
GPR	ground penetrating radar
HAZWOPER	Hazardous Waste Operations and Emergency Response
IP	induced polarization
µg/L	micrograms per liter
mS/cm	micro-Siemens per centimeter
NaBr	sodium bromide
NAWC	Naval Air Warfare Center
ORP	oxidation reduction potential
OTV	optical televiewer
PI	Principal Investigator
PNNL	Pacific Northwest National Laboratory
PVC	polyvinyl chloride

REV	representative element volumes
SC	fluid specific conductance
SP	self-potential
TCE	trichloroethylene
USGS	U.S. Geological Survey
VC	vinyl chloride
VOC	volatile organic compound
WS	water sample

ACKNOWLEDGEMENTS

The following individuals and organizations contributed to this demonstration project:

- Lee Slater (Principal Investigator [PI]), Dimitrios Ntarlagiannis (co-PI), and Judy Robinson (PhD candidate) all from Rutgers University, Newark;
- Fred Day-Lewis (co-PI), John Lane (co-PI), and Carole Johnson all from Office of Groundwater – Branch of Geophysics, United States Geological Survey, Storrs, Connecticut;
- Tim Johnson (co-PI) of Pacific Northwest National Laboratory (PNNL);
- Allen Shapiro (co-PI), United States Geological Survey, Reston, Virginia;
- Claire Tiedeman, United States Geological Survey, Menlo Park, California; and
- Dan Goode, Pierre Lacombe, and Tom Imbrigiotta all from United States Geological Survey, W. Trenton, New Jersey.

Preparation of this report was led by Slater, Robinson, Day-Lewis, and Johnson.

Technical material contained in this report has been approved for public release.
Mention of trade names or commercial products in this report is for informational purposes only;
no endorsement or recommendation is implied.

This page was left blank intentionally.

EXECUTIVE SUMMARY

OBJECTIVES OF THE DEMONSTRATION

Contaminated sites in fractured rock are particularly difficult and expensive to remediate, because characterization and monitoring is problematic in the presence of extreme heterogeneity. The performance objectives of this demonstration focused on evaluating: 1) fracture network characterization using a fractured rock geophysics toolbox (FRGT); 2) autonomous monitoring of amendment delivery and subsequent contaminant biodegradation using geophysical technologies that sense beyond the borehole; 3) application of an 'informed inversion strategy' to improve the geophysical imaging of fractured rock settings relative to what can currently be achieved with off-the-shelf functionality. Specific performance objectives were largely met, although the physical characteristics of the primary demonstration site, being the Naval Air Warfare Center (NAWC) in W. Trenton (New Jersey), limited the performance of some methods in the FRGT. The primary benefit of the FRGT is the ability to provide information on variations in physical properties and the fate of amendment injections into fractured rock beyond the vicinity of local borehole observations. The potential impact on U.S. Department of Defense (DoD) operations relates to improved management decisions that can result from an improved understanding of flow and transport processes at fractured rock site, particularly the effectiveness of amendment treatments in targeting contaminants of concern.

TECHNOLOGY DESCRIPTION

In the FRGT, geophysical characterization data are fed into the processing of geophysical monitoring datasets in order to provide appropriate constraints on the inversion and regularization of the data/images resulting in predictions of the transport of amendments and/or progress of biodegradation beyond the vicinity of boreholes. The characterization data include information from established borehole logging instruments that provide high resolution information on physical properties close to the borehole and less established between borehole imaging methods that capture the continuity of structures beyond individual boreholes. The FRGT incorporates multiple geophysical techniques as it is based on the fundamental premise that there is no silver bullet with respect to geophysical technologies and that multiple methods must be tested at a particular site to determine the ones that will provide the most information beyond the boreholes. At the NAWC demonstration site, the most effective technology for characterization and monitoring beyond the borehole was cross-borehole electrical resistivity tomography (ERT). The performance objectives associated with informed inversion therefore focused on advancing the utility of ERT for characterization and monitoring in fractured rock subject to constraints provided by other technology components of the FRGT.

DEMONSTRATION RESULTS

The demonstration focused on characterization and monitoring using a dense array of seven boreholes each drilled through ~70 feet of unweathered rock. A critical part of the demonstration was the design, development, and testing of a first-of-its-kind integrated array containing electrodes, packers, and injection/sampling ports. This array was constructed to demonstrate in situ ERT monitoring of amendment injections/longer term biodegradation occurring in fractured rock whilst maintaining hydraulically and electrically isolated intervals in all seven boreholes. The demonstration also advanced the functionality of E4D (4D electrical resistivity tomography

forward and inverse modeling code), a high-performance computing code for the inversion of large ERT datasets. Advancements focused on implementation of new regularization constraints that favor site conditions in fractured rock and provide flexibility for incorporating information on the boreholes. Limited laboratory studies were performed to determine the most favorable (from an ERT imaging perspective) amendment substrate from the candidates highlighted as effective at the site. The field demonstration primarily focused on an intensive multi-method downhole and crosshole geophysical characterization campaign followed by a suite of tracer tests and a longer term amendment injection that were imaged with ERT.

The FRGT produced an unprecedented image revealing the continuity of relatively permeable zones within approximately 600 cubic meters (m^3) of rock. The images resolve the alternating sequence of laminated and massive mudstones at the site and the results are validated by borehole logging and crosshole hydraulic testing datasets. Time lapse ERT monitoring was able to monitor the evolution of injected tracers and amendments within targeted fracture zones that control the flow and transport characteristics of this site. The time-lapse ERT images capture strong evidence for channelized flow occurring within the fracture zone and provide unique information on the efficacy of targeted amendment emplacement. The images also offer the possibility of estimating fracture surface area impacted by an amendment treatment, with direct implications for the performance of such remediation treatments with respect to remediation goals. Limited testing of the FRGT at a second site, the Eastland Woolen Mill, Corinna, Maine, highlighted the potential benefits of directional cross borehole ground penetrating radar (DBHGPR) for imaging the continuity of major fracture zones beyond borehole walls.

IMPLEMENTATION ISSUES

Most of the technologies explored in the FRGT are not subject to any specific regulations beyond what is typical for working in boreholes at contaminated sites and acquiring samples. However, continuous open holes are needed for ERT to be effective in fractured rock. Some states regulate the length of open holes to prevent cross contamination between multiple fractures or aquifers connected to the borehole. In this study, a deviation was readily obtained from the state. The specific borehole technology developed in the course of this research—centered on integrated electrode/sampling/packer arrays—helped to address the open-hole regulatory implementation issue, as fractures were hydraulically isolated during tracer experiments and electrical monitoring. Metal borehole casings would prevent the effective use of most geophysical techniques included in the FRGT, although some of the tools in the FRGT can operate effectively though polyvinyl chloride (PVC) casing.

This demonstration involved an extensive technology transfer effort where end-user concerns were specifically addressed through lectures, field demonstrations, and hands-on question and answer sessions with individuals. In total, our tech-transfer courses directly engaged 230 remediation professionals and regulators via short courses approved for continuing education credits. These efforts revealed that end users were typically poorly equipped to make informed decisions about the likely appropriateness of specific components of the FRGT, based on the conditions of a particular site. In order to address this implementation issue, an Excel-based decision support tool was developed to provide recommendations for the selection of specific geophysical techniques for a given project objective and subject to the constraints imposed by the site conditions.

1.0 INTRODUCTION

1.1 BACKGROUND

Geophysical imaging technologies have the potential to provide cost effective, non-invasive techniques for imaging physical properties and transport processes beyond the borehole. Specifically, these technologies may (1) characterize structures controlling flow and transport beyond the borehole; and, (2) diagnose likely changes in pore fluid chemistry within fractured rock associated with amendment delivery and resulting biodegradation that can be verified using a limited (in scope and expense) direct measurement method. Technologies are required to provide site managers with the information necessary to better determine fracture geometries away from wells, fracture connectivity, and the progress of amendment treatments targeting dense non-aqueous phase liquids (DNAPL) within fractured rock. Such information will ultimately assist decision-making regarding the viability of amendment treatment as a remediation option in fractured rock; identification of critical target zones for delivery of amendment treatments; and variations in amendment frequency needed to optimize remediation.

The motivation for this project was that the proposed technology would result in far fewer wells being required to understand the major connected fracture networks dictating flow and transport of an amendment (and subsequent biodegradation induced) in a fractured rock environment. The drilling of fewer wells will reduce direct contact with contaminants, and minimize the problem whereby boreholes act as preferential pathways for contaminant transport between vertically separated fractures thereby facilitating greater transport of contaminants away from the source zone. Furthermore, geophysical technologies could lead to significant cost savings not only as a result of the need for fewer wells, but also as a result of reduced monitoring requirements (e.g., wells, samples, analyses) required to determine the progress of amendment treatments.

1.2 OBJECTIVES OF THE DEMONSTRATION

The overall objective of this project was to demonstrate a method for characterization and monitoring of amendment delivery and subsequent biodegradation of DNAPL (including free and dissolved phase) in fractured rock aquifers based on a fractured rock geophysical toolbox (FRGT). Specific technical objectives of the project included demonstrations of fracture network characterization using geophysical methods sensitive to fracture strike and dip patterns and spanning a wide range of measurement scales; minimally invasive autonomous monitoring of proxies of the timing and extent of amendment delivery and/or DNAPL degradation in fractured rock using combined geophysical and geochemical measurements sensitive to amendment concentration and biodegradation; and the application of “informed” inversion to produce estimates of fracture location, distribution, and orientation with better resolution than is currently possible with commercially available tools.

1.3 REGULATORY DRIVERS

The demonstration (including both the application of the FRGT and verification) was designed to provide end users with the information needed on both the performance of the method (and specific FRGT components) in fractured rock, as well the associated issues regarding spatial and temporal resolution and costs. Tech transfer efforts were integral to the project and designed to give end

users the information needed to make informed decisions on future applications of this technology. In order to receive guidance with such efforts, Kathy Davies, U.S. Environmental Protection Agency (EPA) Region 3, was consulted early in the project to promote introduction of the information generated under this demonstration to groundwater science personnel in regulatory agencies.

2.0 TECHNOLOGY

2.1 TECHNOLOGY DESCRIPTION

This project set out to demonstrate the performance of a FRGT as it is summarized in the overall schematic of the technology shown in Figure 1. In the FRGT, geophysical characterization data are fed into the processing of geophysical monitoring datasets in order to provide appropriate constraints on the inversion and regularization of the data/images resulting in predictions of the transport of amendments and/or progress of biodegradation beyond the vicinity of boreholes. The technology is directed towards acquiring reliable information on structures, amendment delivery, and longer term geochemical transformations beyond boreholes; thus, beyond the range of conventional sampling methods. The technology offers the potential to provide spatially continuous information that reduces the challenges of uncertain interpolation based on sparse datapoints in boreholes. It also presents an opportunity to acquire data at a scale more typical of the heterogeneity controlling flow and transport in the subsurface, in contrast to small scale point measurements made in boreholes.

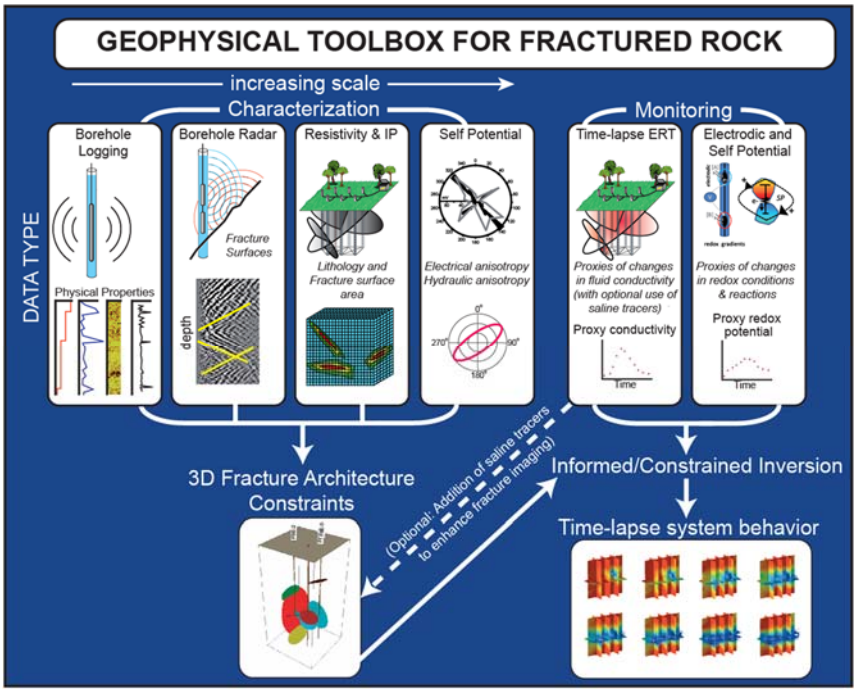

Figure 1. Summary schematic of the FRGT technology.

The FRGT incorporates multiple geophysical techniques as it is based on the fundamental premise that there is no silver bullet with respect to geophysical technologies and that multiple methods must be tested at a particular site to determine the ones that will provide the most information beyond the boreholes. Significant redundancy is integrated into the FRGT in that not all the methods will be utilized in full development of a site characterization and monitoring strategy as described here. Electrical resistivity tomography (ERT) was found to be the most valuable geophysical property at the project demonstration site and therefore is the focus of this cost and performance summary.

The monitoring toolkit of the FRGT exploits geophysical measurements with recognized sensitivity to pore fluid conductivity and redox chemistry at contaminated sites. The ERT method is well suited for tracking changes in bulk conductivity resulting from changes in groundwater chemistry associated with amendment delivery and/or accompanying DNAPL degradation (Johnson et al., 2010). Resistivity methods have been extensively exploited for obtaining information on discrete fractures and/or fracture density as electrolytic conduction in fractured rock is largely through the fractures (Slater et al., 1997). Electrical resistivity imaging (ERI) has also been used to monitor amendment treatments (Johnson et al., 2010; Johnson et al., 2014) and capture indirect evidence of biodegradation (Slater et al., 2009). ERI has also been used to verify the installation of permeable reactive barriers (Slater and Binley, 2003).

2.2 ADVANTAGES AND LIMITATIONS OF THE TECHNOLOGY

The major advantage of the FRGT is the ability to see beyond the boreholes and into the volume of the subsurface between boreholes. Conventional methods for characterization of fractured rock aquifers and monitoring of amendment delivery and subsequent attenuation most often rely on measurements made in boreholes. Such measurements only provide information local to the borehole. Another major advantage of the technology is that measurements are made at spatial scales that better capture the heterogeneity dictating flow and transport. The greatest benefits of the FRGT stand to be reaped when it is deployed as a low cost temporal monitoring system, whereby successive geophysical surveys will be conducted autonomously over time to track amendment delivery and possibly subsequent biogeochemical alterations associated with attenuation. Coupled with an understanding of the underlying geologic structures, the FRGT has the potential to provide critically needed information on fracture geometries, the spatial distribution of the amendment delivery and resulting attenuation within the usually inaccessible fractures, and rock mass beyond the zone of the borehole. The major limitation of the FRGT is that the geophysical techniques do not provide direct estimates of hydraulic properties and/or changes in aqueous geochemical parameters associated with amendment treatment and subsequent contaminant attenuation. However, when used in conjunction with a limited set of direct measurements in boreholes, the geophysical proxy measurements of fluid and rock properties beyond the boreholes have the potential to improve understanding of the spatial distribution of fracture and rock properties as well as the spatial and temporal changes in fluid properties.

3.0 PERFORMANCE OBJECTIVES

Specific performance objectives related to each tool within the FRGT include data to be used and evaluated with respect to meeting the objectives, and the definition of what constitutes success, as is described below and summarized in Table 1. Evaluation of the performance objectives was largely based on comparison of metrics of the soft geophysical datasets with hard data available from established methods that provide high-resolution hard data local to the borehole. The project team capitalized on ongoing U.S. Geological Survey (USGS) research and sampling efforts, and aligned this work with other ongoing projects at the demonstration site. Sampling followed USGS protocols and was performed by USGS staff not included as Principal Investigators (PI) or co-PIs on this project. The hard data on fracture densities and distributions required to conduct validation tests on the characterization component of the FRGT came from borehole geophysical logging datasets collected as part of this demonstration project, supplemented with preexisting site data made available to the project team. The data required to perform blind validation tests on the monitoring component of the FRGT were primarily groundwater samples acquired during and after tracer or amendment injection.

Table 1. Summary of primary performance objectives, associated data requirements and success criteria as defined in the demonstration plan performance objective.

Objective	Data Requirements	Success Criteria	Degree Met
Fracture Network Characterization			
Quantitative performance objective			
Identify strikes, dips, and connectivity of fractures away from boreholes	BHGPR combined with borehole logging data	Fracture dip identified by GPR within 5% of actual dip observed with borehole logging in boreholes. Fracture strike identified by GPR within 5% of actual dip observed with borehole logging in boreholes.	Partly
Qualitative Performance Objective			
Determine distribution of transmissive and connected fractures (away from boreholes) above a threshold	Resistivity imaging and DBHGPR during tracer injection combined with flow meter logging	Accurate grouping of fractures into transmissive or non-transmissive, based on threshold consistent with flow meter logs. Statistics: *non-linear analysis e.g. Markov-Bayes hardness*	Fully
Autonomous Monitoring of Amendment Delivery and/or Biodegradation			
Quantitative Performance Objective			
Measure distribution of injected amendments away from boreholes	ERI combined with ground water sampling (specific conductance) from boreholes	Electrical conductivity changes predicted in the images at boreholes consistent with specific conductance changes recorded in boreholes. *Statistics: correlation analysis*	Fully
Measure redox gradient changes away from boreholes	SP and electrodic potential measurements combined with ORP measurements in boreholes	Direction and magnitude of redox changes correct as compared to borehole analyses.	Procurement issues prevented implementation

Table 1. Summary of primary performance objectives, associated data requirements and success criteria as defined in the demonstration plan performance objective (continued).

Objective	Data Requirements	Success Criteria	Degree Met
Qualitative Performance Objective			
Infer distribution of primary geochemical parameters of interest (e.g., chloride, TCE)	Resistivity and induced polarization measurements combined with geochemical analysis of groundwater samples	Demonstrate correlation of geochemistry with resistivity and induced polarization *Statistics: ANOVA and multiple regression*	Partly
Determine timing of changes in redox potential distribution driven by biodegradation away from boreholes	SP combined with redox chemistry from groundwater sampling and ORP measurements	Demonstrated correlation of geochemistry with resistivity and SPs *Statistics: ANOVA and multiple regression*	Procurement issues prevented implementation
Application of "Informed" Inversion to Improve Imaging of Fractured Rock			
Qualitative Performance Objective			
Optimized high-resolution imaging of fractured networks	Resistivity and induced polarization inversion combined with DBHGPR and borehole logs to define appropriate regularization constraints for fractured rock systems Model predictions from Inverse codes developed under this project and those predictions obtained from commercially available existing software (e.g., Res2DInv)	Improved resolution of fracture networks when using inverse codes developed under this project relative to existing commercial codes. Validation of improvement using synthetic model scenarios based on NAWC (where true model is known) as well as field data acquired at NAWC	Fully
Optimized high-resolution imaging of spatial extent and timing of amendment delivery and subsequent attenuation	Resistivity and SP inversion combined with DBHGPR and borehole logs to define regularization constraints Model predictions from Inverse codes developed under this project and those predictions obtained from commercially available existing software (e.g., Res2DInv)	Improved resolution of amendment distribution and attenuation using inverse codes developed under this project relative to existing commercial codes. Validation of improvement using synthetic model scenarios based on NAWC (where true model is known) as well as field data acquired at NAWC	Partly

ANOVA = analysis of variance
BHGPR = borehole ground penetrating radar
DBHGPR = directional cross borehole ground penetrating radar
GPR = ground penetrating radar
NAWC = Naval Air Warfare Center
ORP = oxidation reduction potential
SP = self-potential
TCE = trichloroethylene

Not all performance objectives defined in the demonstration plan were met, partly because some components of the FRGT did not perform well given the particular geological conditions of the performance site. This was expected and underscores the importance of adopting a toolbox

approach to fractured-rock characterization and monitoring. It was necessary to focus on the components of the FRGT evaluated to have the highest chances of success at the demonstration site. Table 1 summarizes the primary performance objectives defined in the Demonstration Plan for the project, associated data requirements and defined success criteria used to confirm successful performance of individual toolbox components.

4.0 SITE DESCRIPTION

The primary study site for this demonstration was the former NAWC, located in West Trenton, New Jersey (NJ), which was used as a facility to test jet engines from 1955-1998. This site is representative of hundreds of contaminated sites in the eastern United States and thus the lessons learned here are potentially applicable to other fractured sedimentary sites. The fractured bedrock aquifer at the site was extensively contaminated with the chlorinated solvent TCE during operations and presently fractures and the rock matrix are contaminated with TCE and its biotic degradation products cis-dichloroethylene (cDCE) and vinyl chloride (VC).

4.1 SITE LOCATION

NAWC is located at the corner of Jack Stephen Way and Parkway Avenue in West Trenton, NJ (Figure 2). The location of demonstration boreholes 83-89BR (described later) was in between a driveway for an abandoned industrial building that formerly housed jet engines for flight testing and a dirt roadway. The topography is flat with low lying vegetation consisting mostly of long grasses. The site is easily accessible with a regular vehicle via Parkway Avenue.

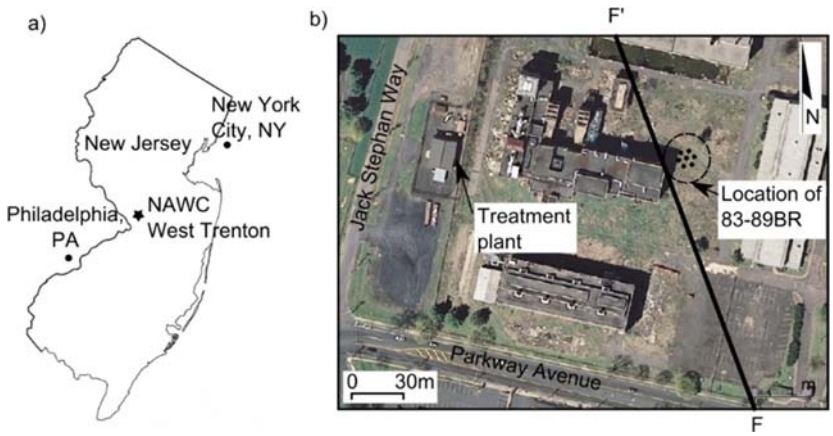

Figure 2. NAWC site location.

4.2 SITE GEOLOGY/HYDROGEOLOGY

The site consists of fractured sedimentary rocks of the Newark Basin. Competent rocks are primarily mudstones and sandstones of the Lockatong and Stockton Formations. Fill, weathered silt, and silty-clay saprolite are underlain by moderately-dipping alternating massive and laminated mudstone units, which contain highly fractured black carbon-rich units (Figure 3) (Lacombe & Burton, 2010; Tiedeman et al., 2010). This study focused on the unweathered mudstone units where dominant flow pathways identified from hydraulic testing are through a series of cross-cutting faults and discrete fracture zones associated with the carbon rich intervals (Lacombe & Burton, 2010; Ellefsen et al., 2012).

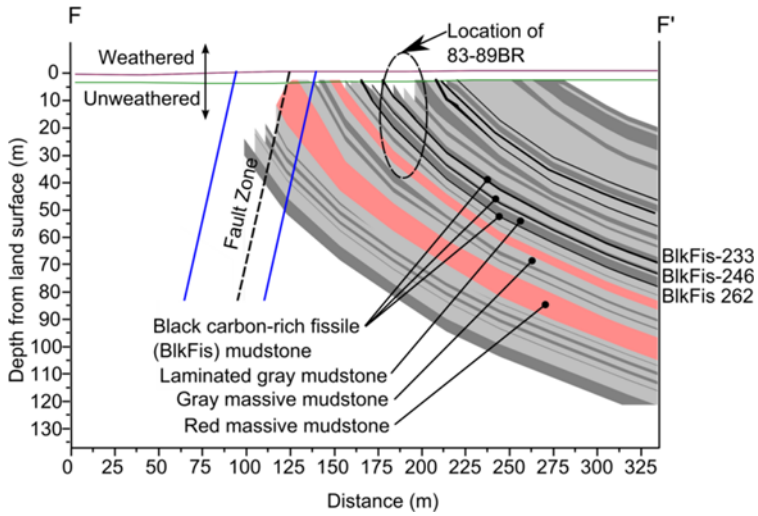

Figure 3. Section F-F (see Figure 2) showing geologic cross section in the vicinity of 83-89BR boreholes.
(from Robinson et al, 2015)

4.3 CONTAMINANT DISTRIBUTION

Peak chlorinated volatile organic compound (CVOC) concentrations (in micrograms per liter [µg/L]) for wells in the vicinity of 83-89BR on the NAWC site are shown in Figure 4. These concentrations were computed as the molar sum of peak concentrations of 'original TCE' consisting of TCE, cDCE, and VC. The data for this figure were collected from 1990-2014. Figure 5 shows the spatial extent of the contamination as well as the irregularity of concentrations of the plume, hence highlighting the complex fracture networks in fractured rock.

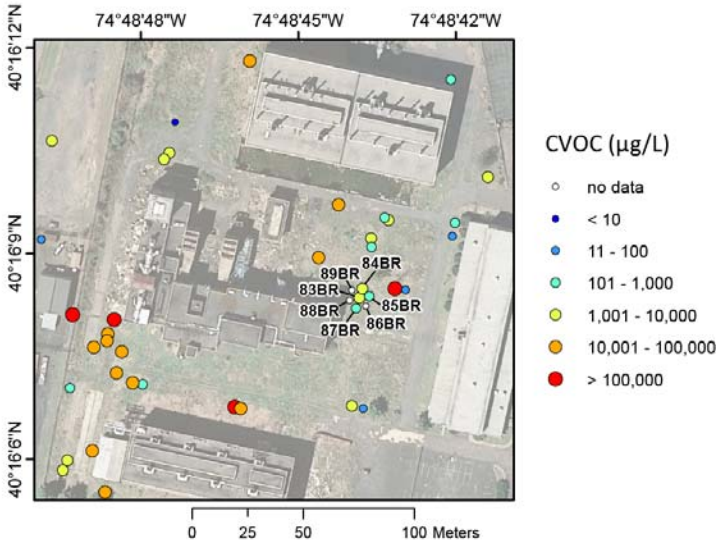

Figure 4. Peak molar concentrations of original TCE at wells in the vicinity of 83-89BR for samples collected between 1990-2014.
(revised from Goode, et al., 2014)

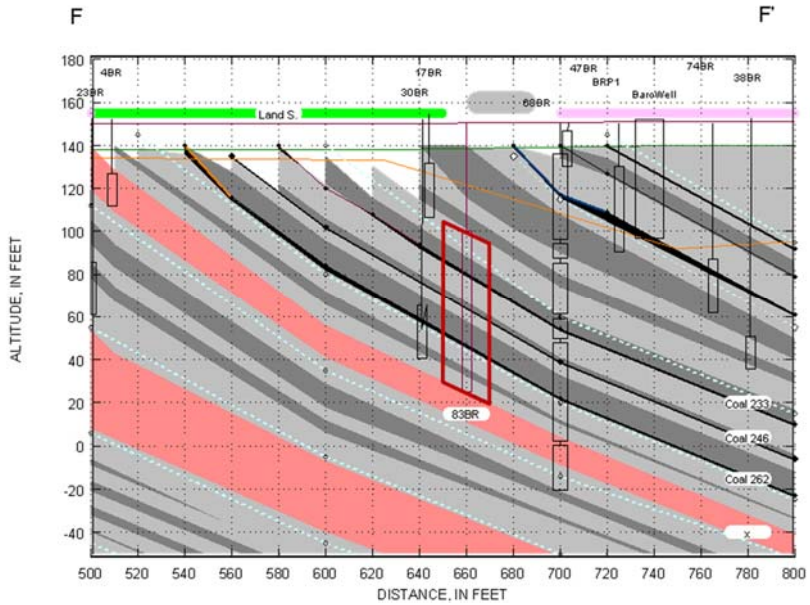

Figure 5. Cross section F-F' showing the selected region bounded by the array of boreholes selected for this demonstration.

The region targets three fractured zone intervals and focuses on a heavily contaminated unweathered zone.

This page was left blank intentionally.

5.0 TEST DESIGN

5.1 CONCEPTUAL EXPERIMENTAL DESIGN

This demonstration was based on a study of an approximately 1400 m^3 volume of fractured rock defined by seven boreholes that were drilled at the NAWC site. The targeted rock volume was selected to intercept multiple permeable bedding plane features known to be contaminated with TCE (Figure 5). The operational phases of the demonstration included: drilling/coring; borehole geophysical logging; cross-borehole geophysical imaging of rock structure; and preliminary tracer tests followed by cross-borehole time-lapse monitoring of a sequence of tracer tests that ended with a monitored amendment injection. The core and geophysical logging data were acquired to provide hard data to evaluate the performance of the cross-borehole geophysical imaging and monitoring effort that formed the backbone of this demonstration. The core and logging data were also used as constraints in the demonstration of an informed inversion framework required to improve the performance of the cross-borehole geophysical technologies in imaging a fractured rock system. A preliminary tracer test was performed to determine key parameters needed to constrain the design and implementation of the geophysical monitoring tracer tests. The experiment design included the construction of first-of-a-kind borehole infrastructure for conducting continuous geophysical monitoring into fractured rock during the injection of tracers into hydraulically isolated intervals of the rock mass.

5.2 BASELINE CHARACTERIZATION

5.2.1 Drilling, Coring and Well Installation

Seven boreholes, designated sequentially 83BR through 89BR, were drilled along strike in a wagon wheel pattern (Figures 6 and 7). Distances between boreholes were designed such that the information content of ERT imaging during tracer/amendment injections could appropriately capture injection evolution beyond the borehole. At these inter-borehole distances, standard hydraulic testing methods such as borehole water sampling, borehole geophysical logging, and/or hydraulic testing can provide valuable supporting information.

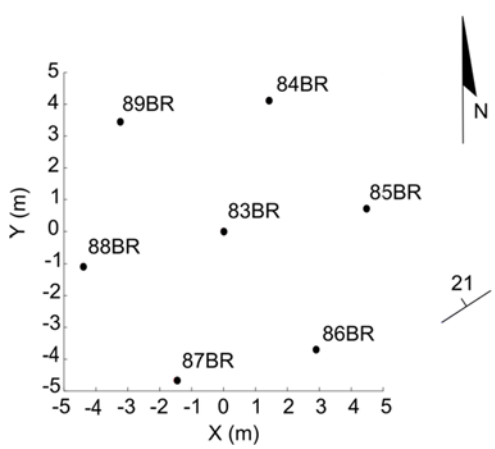

Figure 6. As-built borehole schematic.

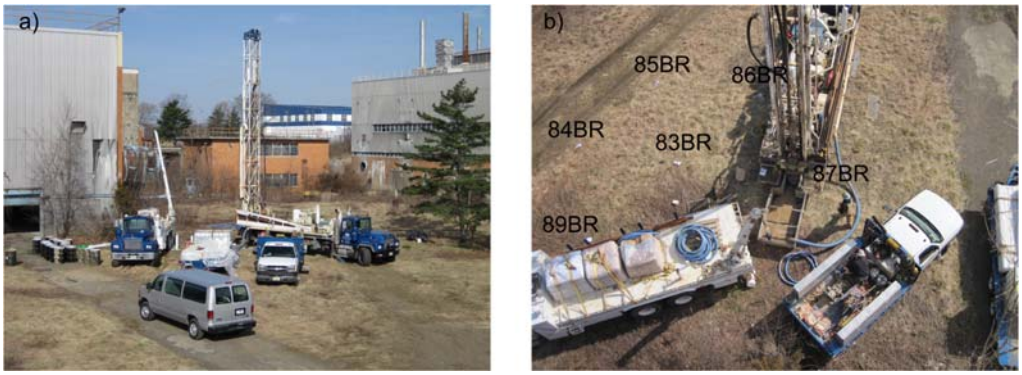

Figure 7. Drill rig and site view (a), and aerial photo showing drilling locations (b).

A 10-inch (25 cm) borehole was drilled within the top weathered units. This was lined with a 6-inch (15 cm) polyvinyl chloride (PVC) casing sealed into place with bentonite. A surface steel casing was then grouted into place (Figure 8). Drilling depths of 10-inch (25 cm) diameter well sections ranged from 12.50 – 15.85 meters below land surface (bls). Below the weathered rock, a 3.8-inch (10 cm) core bit was used. Cores were catalogued and chiseled samples were selected for further volatile organic compound (VOC) analysis. Rock core samples were collected and preserved in the field. After bringing the core barrel to the surface, samples were selected near suspected permeable features and from unfractured strata between permeable features.

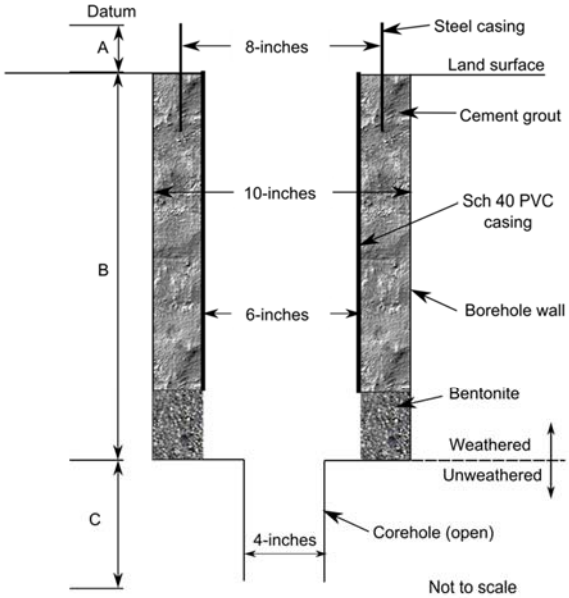

Designation	Description	83BR	84BR	85BR	86BR	87BR	88BR	89BR
A	Landsurface, LS	0.90	0.90	0.90	0.87	0.84	0.80	0.88
B	Bottom of 10 in borehole below LS	14.94	15.85	14.94	12.50	12.50	14.02	15.85
C	Length of open 4 in interval	17.02	19.25	17.17	20.77	20.71	22.45	20.31
	Length of core*	21.34	21.95	21.34	22.25	22.25	21.95	21.95

* Partial collapse of the 4 in interval resulted in the length of the core being larger than the length of the open 4-in interval

Figure 8. Borehole section view for 83-89BR wells.

Coring depths were such that three known highly fractured carbon units were penetrated, being designated BlkFis 233, BlkFis 246, and BlkFis 262 (Figure 5). Uncased 3.8-inch (10 cm) intervals ranged from 17-22.5 meters in length. Depth to bottom of borehole bls ranged from 32-36.5 meters.

This demonstration ultimately focused on tracer and amendment injection monitoring into a series of cross cutting faults, which were found to be highly transmissive in cross borehole hydraulic testing.

5.2.2 Geophysical Logging

Borehole geophysical logging constituted the major source of a priori information to be used in boreholes 83BR-89BR to constrain electrical resistivity imaging. Standard logs and specialized logs collected within each borehole are shown in Table 2.

Table 2. Borehole logging methods used in 83BR-89BR.

METHODS	83BR	84BR	85BR	86BR	87BR	88BR	89BR
Gamma	X	X	X	X	X	X	X
Caliper	X	X	X	X	X	X	X
Electromagnetic Induction (EMI)	X	X	X	X	X	X	X
Normal resistivity Spontaneous potential (SP) Single point resistance (SPR)	X	X	X	X	X	X	X
Induced polarization (IP)	X	X	X	X	X	-	X
Fluid temperature and conductivity	*	*	*	*	*	X	*
Heat-pulse flowmeter (FM)	*	*	*	*	*	-	*
Cross-hole FM	X	X	X	X	X	-	X
Optical televiewer (OTV)	X	X	X	X	X	X	X
Acoustical televiewer (ATV)	X	X	X	X	X	X	X
Deviation	X	X	X	X	X	X	X
Neutron	X	X	X	X	X	X	X
Nuclear magnetic resonance (NMR)	X		X		X	-	
Radar (reflection and level)				X	X		

X indicates completed; * indicates ambient and post-stress conditions, - not collected due to borehole liner installation

Borehole logs (acoustical televiewer [ATV], optical televiewer [OTV], caliper) were used to identify fracture intersection depths (Table 2) and Gamma/Normal logs were used to correlate lithologic units within each borehole to aid in the identification of transmissive fracture zones. Borehole deviation logs were used to position each borehole in the ERT modeling. Ambient and stressed conditions were tested using single-hole and cross-hole heat pulse flowmeter tests. Minor ambient flow was recorded in boreholes 83BR, 86BR, 87BR. Cross-hole tests were performed to measure the response of nearby boreholes under stressed conditions when an injection occurs. Interconnections between boreholes could be identified; however, information on individual transmissive fracture zones was limited due to the fact that there was no vertical isolation within each borehole column. Geophysical logs are detailed in the Appendix of the Final Report.

5.2.3 Hydraulic Testing

Cross-borehole aquifer tests were conducted on boreholes 83BR-89BR to infer locations and extents of permeable fractures. These tests were led by Claire Tiedeman of the USGS (Menlo Park, CA). Discrete intervals, determined from the geophysical logs, were bounded by custom-designed packers within each borehole to isolate fracture zones. The same custom-designed low-pressure

packers were also used in the electrode arrays described later. One-hour cross-hole tests were sequentially conducted over 13 intervals. Figure 9 shows the hydraulic connections qualitatively inferred from the drawdown data. Packer zones with similar colors represent hydraulically connected zones, while the line type qualitatively denotes the level of connectivity inferred from the degree of drawdown observed in response to pumping. Packer zones between 83BR, 85BR, and 87BR (solid blue circles) exhibited strong connectivity and were selected as the focus of the tracer studies making up the core of the demonstration described later.

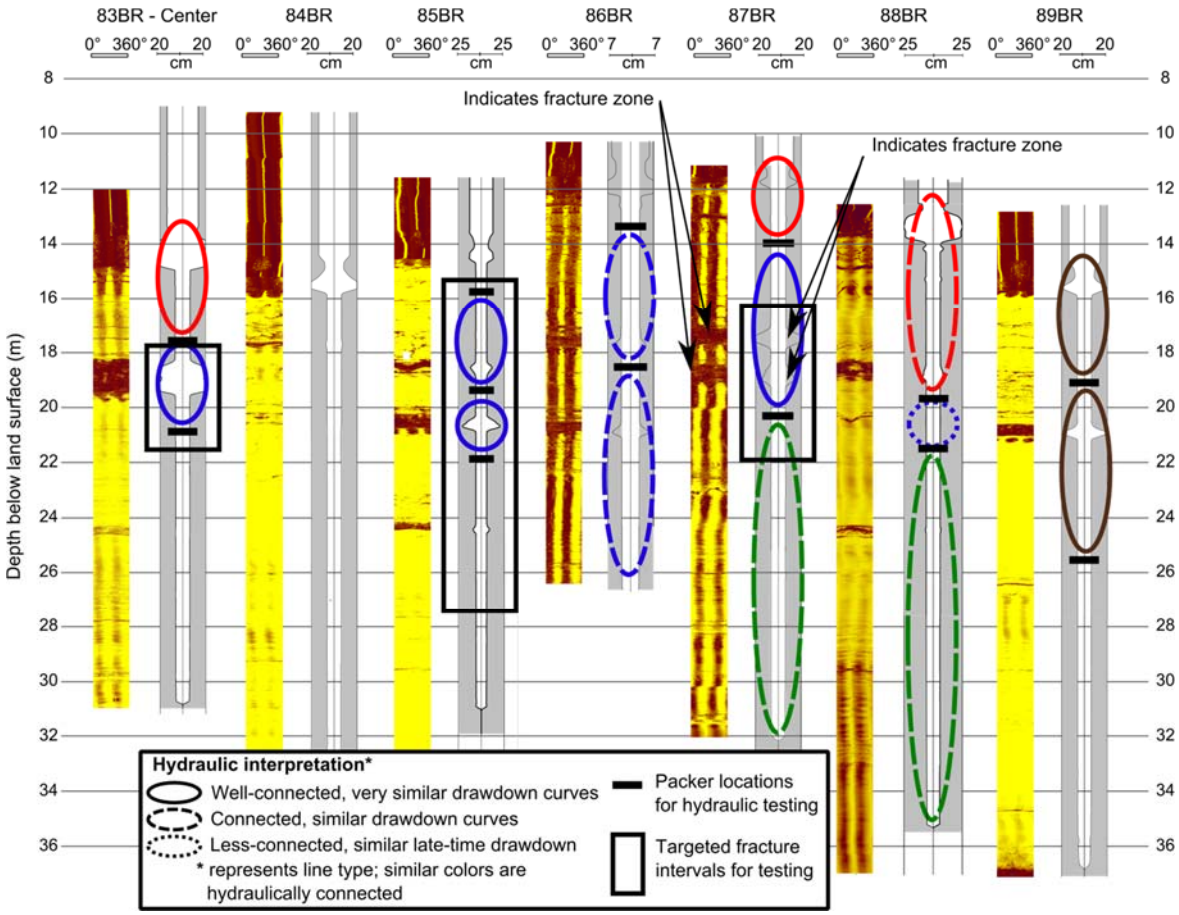

Figure 9. Hydraulic interpretation from drawdown data alongside caliper and ATV borehole logs.

Similar colored ovals represent hydraulically connected packer-isolated borehole intervals. Packer placement for hydraulic testing is shown. There were no packers in 84BR, where negligible open-hole drawdown was detected during all aquifer tests.
Interpretation generated by Claire Tiedeman (USGS, Menlo Park, CA).

5.3 LABORATORY STUDY RESULTS

5.3.1 Amendment Selection Process

The major component of this demonstration project ultimately focused on three dimensional (3D) time-lapse ERT imaging of flow and transport processes of an amendment injection. For time-lapse ERT imaging, it is important that there is a sufficient measurable conductivity contrast between the native groundwater fluid and the fluid spiked with the amendment injection. A

laboratory study was conducted to determine the conductivity contrast of the amendment with native groundwater as a function of increasing concentrations of a substrate; and the calibration curves to potentially convert ERT estimates of electrical conductivity to concentration of substrate (ultimately not done as too uncertain). Native groundwater was extracted from 83BR (0.491 micro-Siemens per centimeter [mS/cm]) to which the mass of the substrate was incrementally added. Molasses had the highest conductivity of the three substrates with a maximum conductivity equal to 18.25 mS/cm, which equates to a conductivity contrast of approximately 37 with the native groundwater. Molasses was therefore used in this demonstration. Sodium bromide (NaBr) was further used to increase the conductivity contrast of the solution.

5.4 FIELD TESTING

5.4.1 Static ERT Characterization

Characterization ERT images are shown as cross sectional slices along borehole boundaries for 87-83-85BR (Figure 10). Additional examples for 88-83-84BR and 89-83-86BR can be found in the Final Report. Electrically conductive zones are shown in red (i.e., higher conductivity) and more resistive zones are shown in blue. The images highlight a structure of alternating conductive and resistive layers oriented similar to alternating massive and laminated beds shown in Figure 3. The results of the coring analysis are shown within each borehole where fracture intersection depths and apertures are marked as black rectangles. Generally, these fracture intersection depths align well with electrically conductive units and lithological boundaries. An electrically conductive pathway is shown between borehole pairs 87BR and 83BR and borehole pairs 83BR and 85BR. This region was chosen as the focus of the tracer and amendment injection studies of the demonstration. In the time-lapse analysis of the ERT data, the characterization dataset shown here was used as the background model.

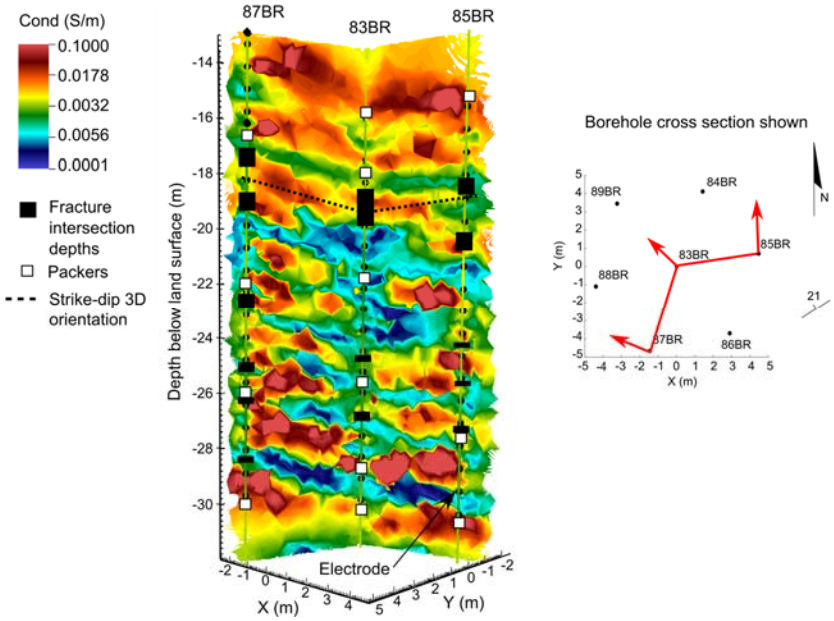

Figure 10. Electrical resistivity image for slice 85-83-87 with fracture intersection depths and packers, and strike-dip 3D orientation.

In order to present an unobstructed view of 83BR, 85BR and 87BR, 86BR is not shown.

5.5 SAMPLING METHODS

5.5.1 ERT Tracer tests and Amendment Injections

5.5.1.1 Overview

The major part of this demonstration focused on showcasing the ability of ERT to capture the progress of amendment injections into fractured rock. The motivation was that ERT has the potential to provide high resolution information on the fate of amendment injections and to provide information on system state changes at relevant scales that integrate the physical property variations controlling flow and transport. A technical challenge was to design an appropriate tracer/amendment strategy that would fully demonstrate the rich information content available from time-lapse ERT. Previous amendment injections at the NAWC site conducted under other Strategic Environmental Research and Development Program funding had highlighted the major uncertainty associated with the delivery of amendments into contaminated fracture zones and the fate of the amendments beyond the boreholes. The following sections describe the two test designs that were most successful, and ultimately resulted in a showcase demonstration of the ability of ERT to resolve amendment delivery at an unprecedented spatiotemporal scale. The Final Report contains details of earlier tests that were unsuccessful.

5.5.1.2 87BR-85BR

An ERT tracer test was conducted between 87BR and 85BR on April 16-18, 2014, and involved two separate fluid injections whereby a conductive tracer injection was subsequently followed by a resistive tracer injection. Tracers were injected in successive pulses using a peristaltic pump, where a pumped injection at 87BR occurred for 5 minutes and then the pump was shut off to collect an ERT dataset. ERT imaging occurred only when the injection pump was off in order to limit temporal smearing over the 20-minute acquisition time. After the entire tracer volume was injected into 87BR, withdrawal from the extraction borehole, 85BR, occurred in the same fashion i.e., in 5 minute pulses, with the pump again turned off between each pulse (Figure 11). Water samples were collected during the pulsed extraction from 85BR. ERT imaging again only occurred when the extraction pump was off. To subsequently remove tracer mass from the system, the extraction borehole (85BR) was pumped for a minimum of 16 hours. During this period, water samples were collected every 10 minutes for 1 hour, then hourly afterwards. Figure 12 presents a flowchart of the 87BR-85BR tracer experiment steps with step numbers denoted in square brackets [ ]. Table 3 contains the specific details of the ERT tracer test for each part of this experiment.

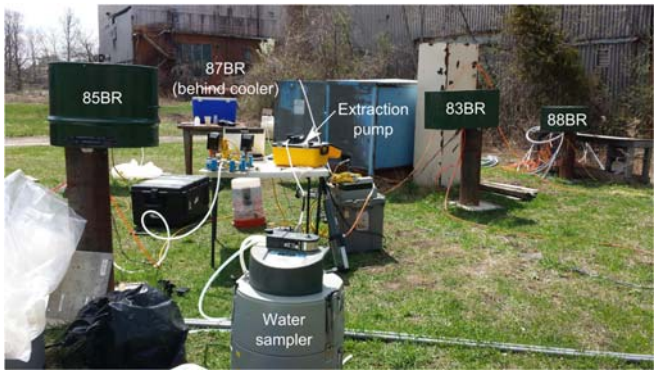

Figure 11. Field set-up for 87BR-85BR tracer test during extraction from 85BR.

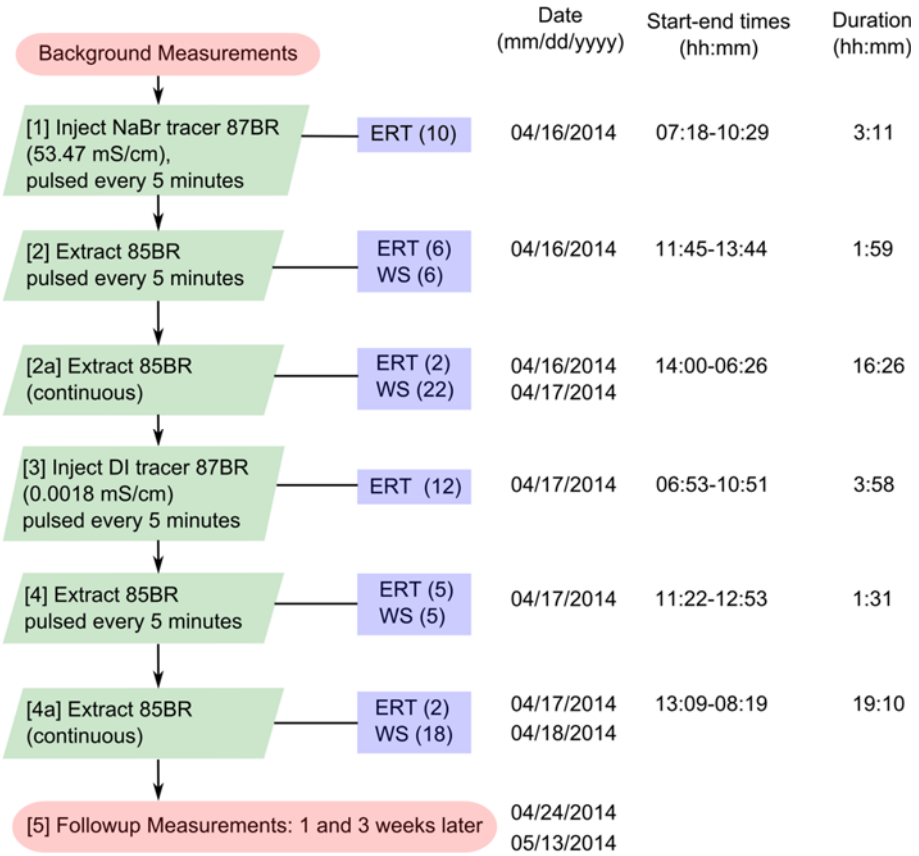

Figure 12. Flow chart of tracer test where numbers of ERT data acquisitions and water samples (WS) are indicated in parentheses ( ).

Table 3. ERT tracer test details for 87BR-85BR.

Description	# Pulsed Injections	Approximate Injection Volume (L)	# Water Samples*	Approximate Extraction Volume (L)
[1] Conductive Injection	9	22	-	-
[2] Conductive Extraction	-	-	6	14
[2a] Extended Extraction	-	-	22	473
[3] Resistive Injection	12	34	-	-
[4] Resistive Extraction	-	-	5	8
[4a] Extended Extraction	-	-	25	674

* For [2] and [4], the # water samples = # pulsed extractions
L = liter

Native groundwater (22 L) was pumped from 87BR and used as the background medium for the conductive tracer injection (step [1] in Figure 12). Based on the high dilution effect observed during earlier tracer tests, a conductivity contrast of 89 was used between the native groundwater (0.60 mS/cm) and tracer solution (53.47 mS/cm). In addition to ERT datasets collected during the nine pulsed conductive injections in (step [1] in Figure 12), another ERT dataset was collected under static conditions shortly after the entire conductive volume was injected. This was followed

by pulsed extraction with acquisition of five ERT data sets (step [2] in Figure 12). Finally, extended extraction (step [2a] in Figure 12) occurred for 16.5 hours.

Deionized water (DI) was subsequently used as a resistive tracer and pulse-injected into 87BR for 12 intervals (step [3] in Figure 12). The fluid specific conductance for the DI water injected was 1.8x10-3 mS/cm, being 333 times more resistive than background concentrations (the true contrast may have been higher due to the presence of residual tracer from the conductive injection). Five pulsed extractions occurred at 85BR after the resistive injection (step [4] in Figure 12). This was followed by 19.17 hours of extraction (step [4a] in Figure 12).

Further ERT measurements (step [5] in Figure 12) were collected 1 and 3 weeks after tracer injection. One week after the tracer test, water was extracted from 85BR for 4 hours to facilitate further removal of tracer mass and to monitor bromide concentrations. Water samples were collected every 5 minutes for the first half hour, then hourly. ERT measurements were collected before and after the extraction. At 3 weeks post-tracer test, only ERT measurements were collected under no pumping conditions.

5.5.1.3 ERT Monitoring of Amendment Injection into 87BR

After successful 3D ERT imaging of tracer migration in the 87BR-85BR tracer test, a similar design was utilized to inject an amendment in 87BR on July 29, 2014. This test differed from previous tracer tests in that there was no planned extraction of fluid from any of the surrounding boreholes; the intention was to leave the injected amendment in-place in order to monitor for electrical changes associated with the possible biodegradation of TCE, cDCE, and VC. Sixty L of native groundwater (0.533 mS/cm) was extracted from 87BR to which sodium bromide (6,134 grams [g]) and molasses (21,876 g) were added to give a fluid specific conductance of 50.2 mS/cm. Seventeen injections were pulsed into 87BR (flowrate=1.2 L/minute) initially at 3 minute intervals with increased injection times corresponding to decreasing heads within the amendment reservoir.

Water samples from within the water sample zones of individual arrays were collected prior to and after the amendment injection in an effort to find evidence for biodegradation surrounding particular boreholes after the injection. Based on the hydraulic testing and flowmeter logging, we expected a response within 87BR, the injection borehole, and hydraulically connected boreholes 83BR and 85BR. Borehole 84BR was also sampled as a control, as we did not expect to see the same trends in key compounds here due to the isolation of this borehole from 83BR, 85BR, and 87BR. Prior water samples were collected on July 9, 2014, or 20 days before the injection; afterwards, samples were collected on August 25, 2014, or 27 days after the injection. Concentrations of key compounds were determined by laboratory analysis including trichloroethylene, cis-1,2-dichloroethene, trans-1,2-Dichloroethene, 1,1-dichloroethene, and VC.

5.6 SAMPLING RESULTS

5.6.1 87BR-85BR

Relative changes in borehole apparent conductivities profiles for 83BR, 85BR, and 87BR (the only boreholes showing significant changes) before and during the four stages of the tracer test are shown in Figure 13, with 86BR shown for comparison. Figure 13 only shows a subset of the datasets collected at the end of step [1] through step [4a] within the ERT tracer test. The largest conductivity changes occur within 87BR and 83BR during the conductive injection. The effect of

the resistive injection is seen in 87BR, with small to insignificant changes occurring in 83BR and 85BR. Extractions from 85BR appear to decrease conductivities in all boreholes (except 86BR).

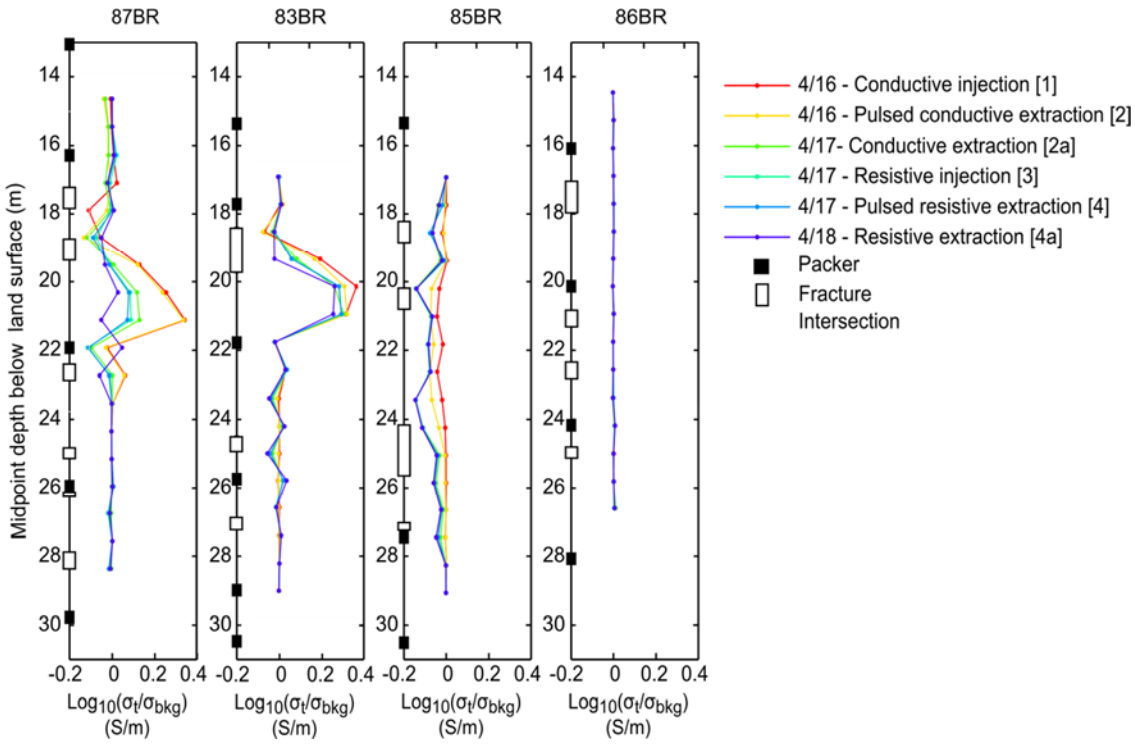

Figure 13. A subset of vertical apparent conductivity depth profiles for wells showing the largest conductivity changes: 87BR, 83BR, 85BR before and during the four-part tracer test.

The response for 86BR (assumed to be unconnected) is shown for comparison.

To determine the minimum isocontour plotted in the time-lapse ERT images in this tracer test, a rigorous approach was taken whereby a synthetic study was performed and forward models were generated from the baseline and final conductive injection inversions. Noise was added to these datasets based on the error model used for the field datasets (described above) and a time-lapse inversion was performed. It was found that random inversion artifacts inconsistent with the migration of the tracer began to appear in the images when the minimum isocontour (of log10 conductivity relative to the background conductivity) was less than 0.035 S m^{-1}/S m^{-1}. Therefore, the project team assumed the ERT inversion detection capability to be equal to 0.035 S m^{-1}/S m^{-1}, representing a change in conductivity equal to 8.4%. All plots therefore show a minimum isocontour equal to this value.

A plan view of the migration of the conductive injection (step [1]) determined from the 3D ERT tracer study is shown in Figure 14, as relative changes from the background conductivity. The largest changes in spatial extent appear after the third injection (Figure 14A-a) and persist until after the final (ninth) injection (Figure 14A-h) and illuminate the migration of a conductive plume from 87BR to 83BR and in the direction of 88BR. Migration of the tracer to 85BR is not implied in these images. The evolution of the vertical extent of the conductive injection is shown in Figure 14B for the same time steps as in Figure 14A. The changes in conductivity are confined to the

targeted fracture zone interval. The conductive plume appears just below the second fracture zone in 87BR (at about 19 meters bls and appears to enter 83BR at the bottom of the top fracture zone (at about 19.5 meters bls).

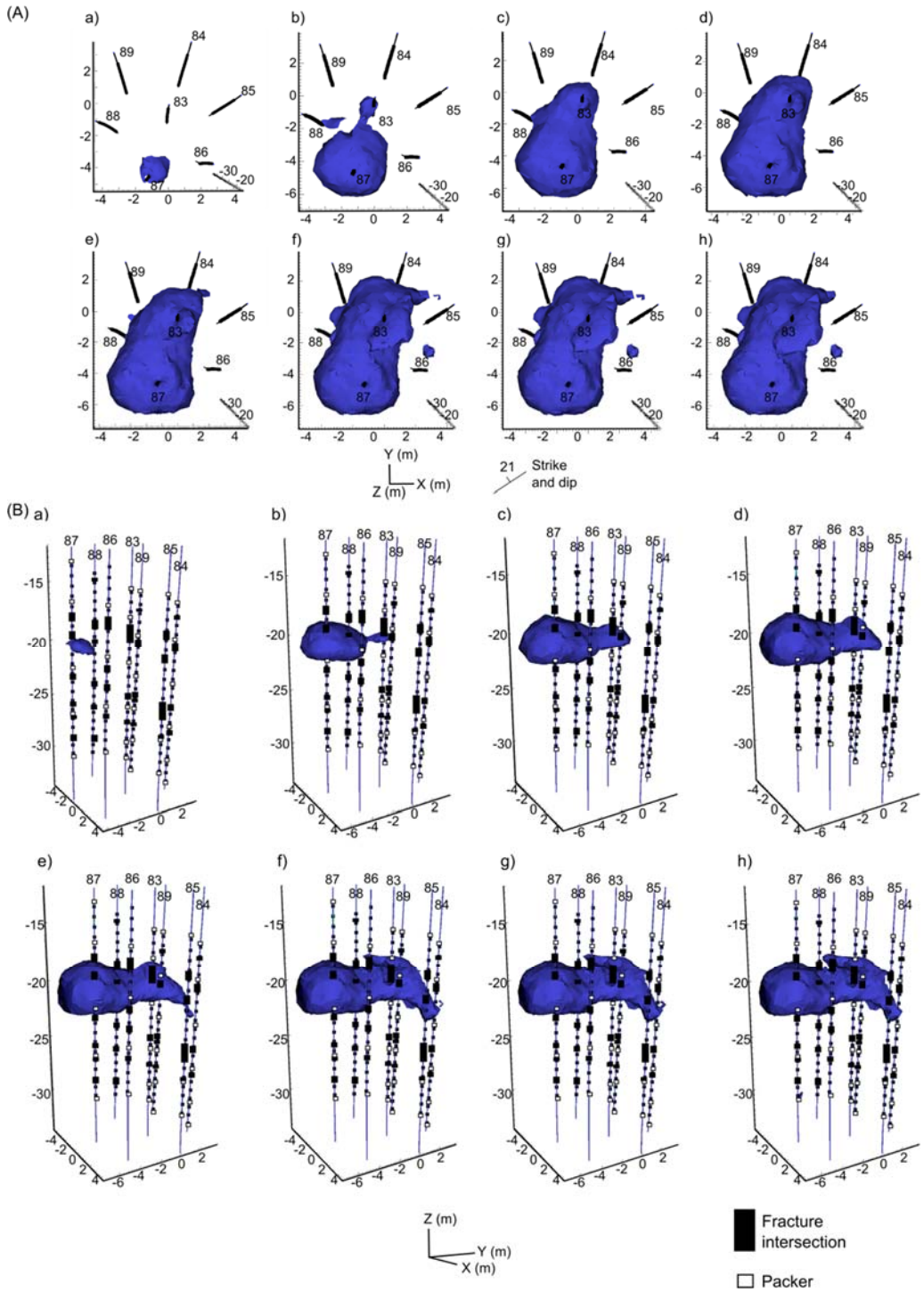

Figure 14. Time-lapse ERT image of relative change in electrical conductivity ($cond_t$ = conductivity at time slice 't', $cond_0$ = conductivity of background) during tracer injection showing (A) plan view (B) elevation view.

Images a-g represent the 2nd to 10th (last) injections. The 7th injection has been omitted due to minor conductivity changes from the previous injection. The isocontour shown is $\log10(Cond_t/Cond_0) = 0.035$.

Figures 15a through 15d show time-lapse images from datasets collected on the same day as the tracer injection tests beginning with the last conductive injection (Figure 15a is the same as part h of Figure 14B). Figures 15b-c show conductivity changes after the first and last deionized water injections, respectively. Figure 15d is for data acquired after 4 hours of extraction pumping from 85BR following the deionized water injection. Note that the resistive injection has little effect on the images shown in Figures 15b-d.

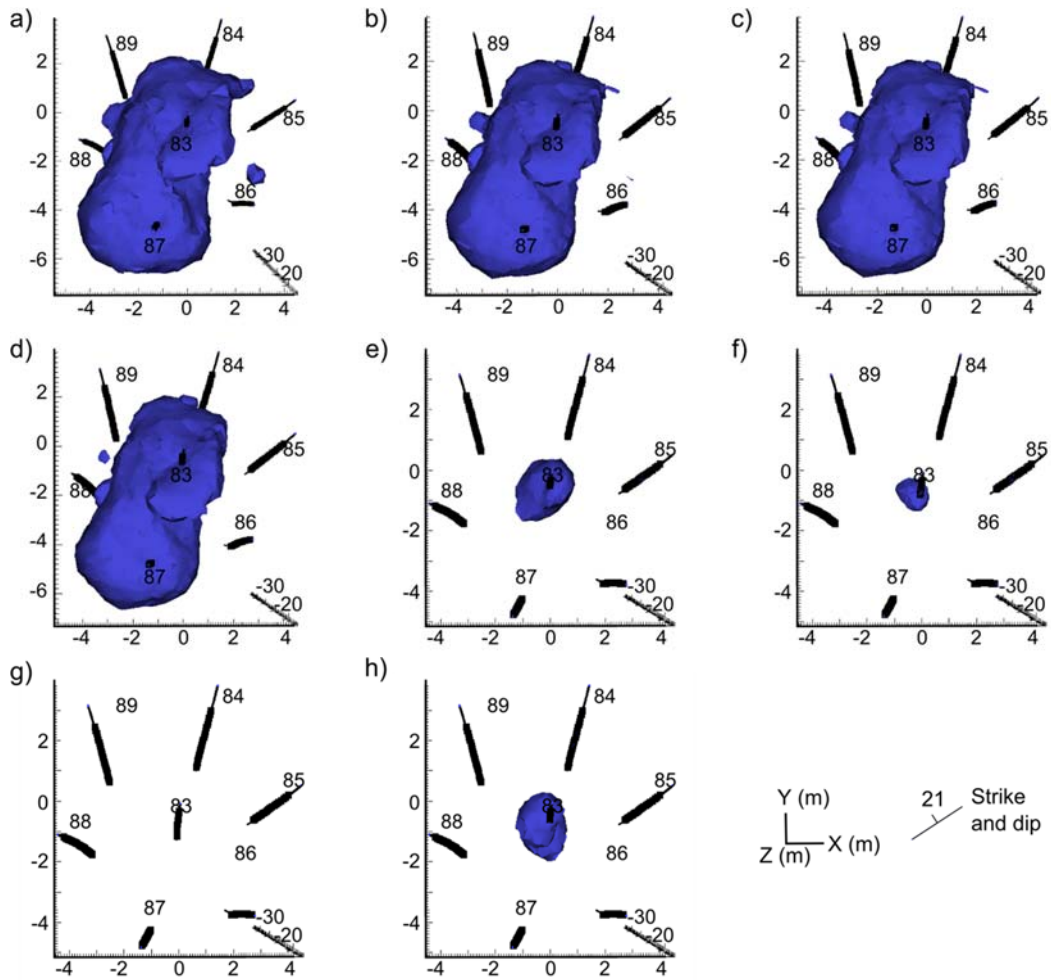

Figure 15. Time-lapse ERT images of relative change in electrical conductivity ($Cond_t$ = conductivity at time slice 't', $Cond_0$ = conductivity of background) following the conductive tracer injection.

a) 30 minutes after the final conductive injection before extraction at 85BR (also shown in Figure 11h); b) 1st DIinjection; c) last DIinjection; d) 4 hours after 85BR extraction following DIinjection; e) 20 hours after 85BR extraction following DIinjection; e) One week following completion of tracer test f) One week following completion of tracer test after 4 hours of extraction from 85BR; f) Three weeks following the tracer test. The isocontour shown is $\log10(Cond_t/Cond_0) = 0.035$.

Following the completion of the tracer test, extraction from 85BR for 20 hours has a dramatic effect on the relative change in conductivity with changes focused around 83BR. (Figure 15e) There was a decrease in the conductive plume surrounding 83BR 1 week following the tracer test

(Figure 15f); after 4 hours of extraction from 85BR (Figure 15g), the plume is no longer visible. However, note that a decreased conductivity contrast between the tracer and the native groundwater due to fluid movement will limit ERT detection. Three weeks after the tracer injections, a conductive plume persists around 83BR in the ERT image (Figure 15h), possibly suggesting back-diffusion of conductive tracer (i.e., from this tracer injection or previous injections) from the matrix into the mobile domain.

This tracer injection experiment provided valuable information at a plot scale appropriate for capturing migration pathways under a pulsed-tracer injection test. The 3D spatial extent of the tracer migration highlights flow and transport within a heterogeneous fractured rock system. The major flow pathways observed, particularly for the conductive injection, are likely in part due to the higher-density of the bromide tracer causing down-dip migration. Available geologic data and the hydraulic connections inferred from the drawdown data are consistent with the migration pathways imaged. The 3D extent of the tracer could not have been resolved using standard borehole geophysical methods or hydraulic testing alone. For example, while the ERT images generally show tracer migration pathways that are down-dip in the direction of strike, more complexity is revealed, particularly surrounding 88BR. The images indicate that a convoluted tracer transport pathway extending close to 88BR exists between 83BR and 87BR. The results indicate that characterizing fractured rock with ERT clearly enhances understanding of tracer transport pathways relative to point measurements from boreholes alone.

5.6.2 Amendment Injection

Following the amendment injection, the vertical ERT profiles exhibit a clear decrease in apparent conductivity (Figure 16). In 87BR, 83BR, and 85BR vertical downward migration of the residual amendment appears likely as evidenced by apparent conductivity increasing at depths below the injection interval over time. Interestingly, 86BR exhibits changes in apparent conductivity below 22 meters depth post-injection, although these changes are small compared to the other surrounding boreholes.

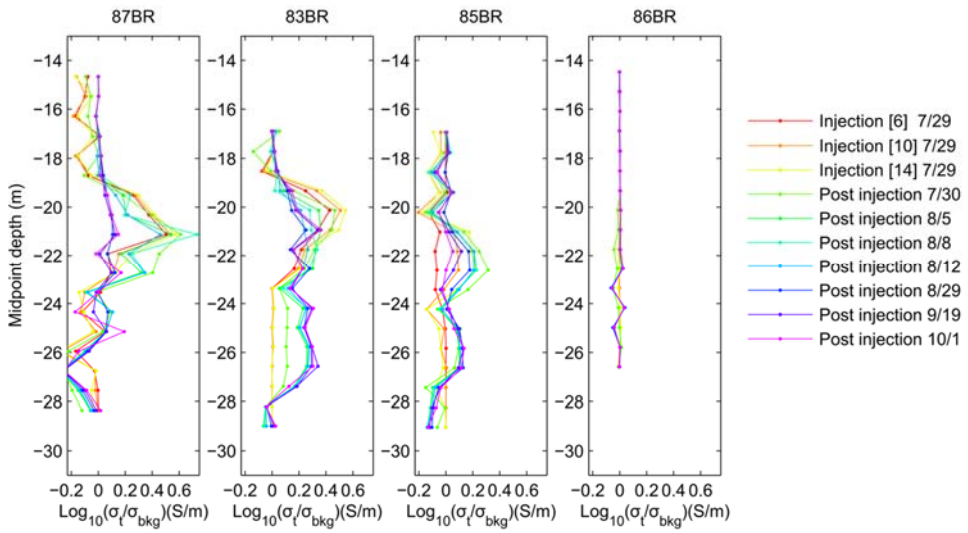

Figure 16. Vertical ERT profiles within injection borehole 87BR and boreholes with the largest conductivity changes, 83BR and 85BR.

Borehole 86BR is shown for comparison. Amendment injection numbers in square brackets [ ] represent the sequential injection number (out of 17 total injections).

Inverted 3D ERT images during-and-post amendment injection (Figure 17 and Figure 18) show the evolution of a conductive plume beginning at the injection borehole (87BR), followed by migration to 83BR and then to 85BR (Figure 17a-d). The most extensive conductivity changes are shown post injection (Figures 17e-f) whilst localized conductivity changes are notable at depth around boreholes 87BR, 83BR, and 85BR. A plan view of the conductivity changes (Figure 18) better shows that these changes are primarily localized around these boreholes and do not extend into the formation. Fourteen days following the amendment injection (Figures 18g and 18g), the highest conductivity changes are at about 29 meters depth in 87BR and between boreholes 83BR and 85BR. These changes are less spatially extensive 64 days following the amendment injection.

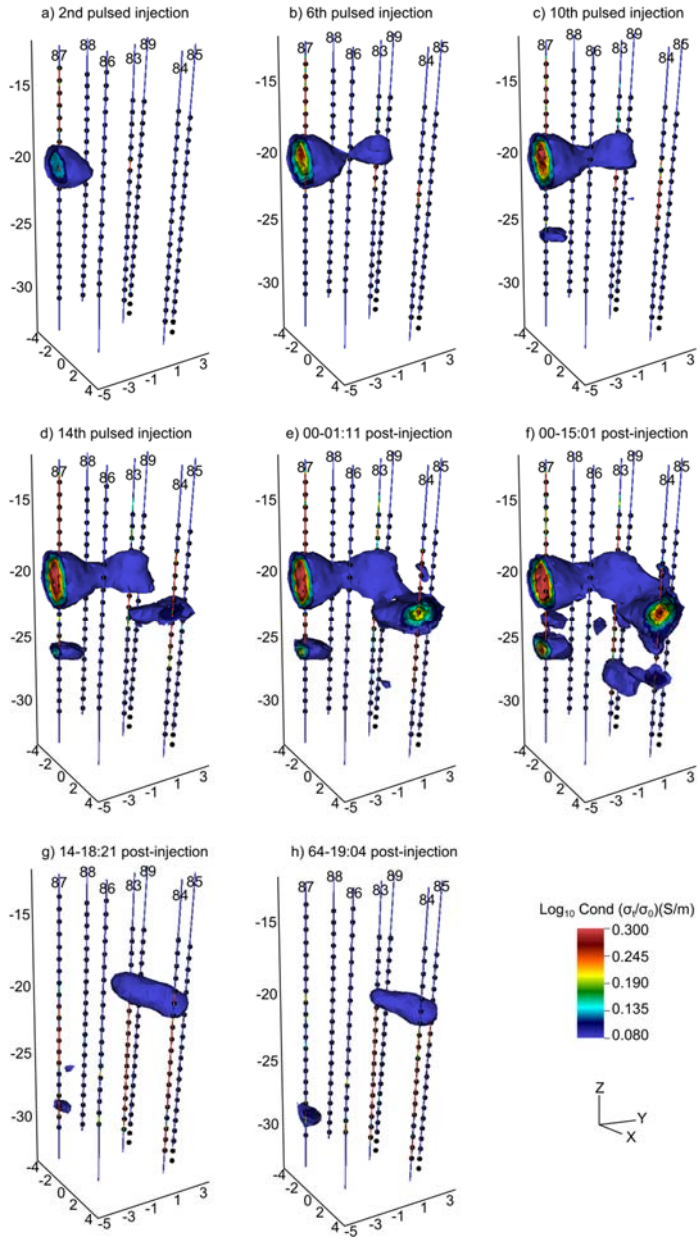

Figure 17. Elevation view of time-lapse 3D ERT conductivity changes during and post amendment injection.

The time formats of the post injection images e) f) g) and h) are dd (days)-hh:mm. One contour equal to 0.08 S/m is used as an image threshold.

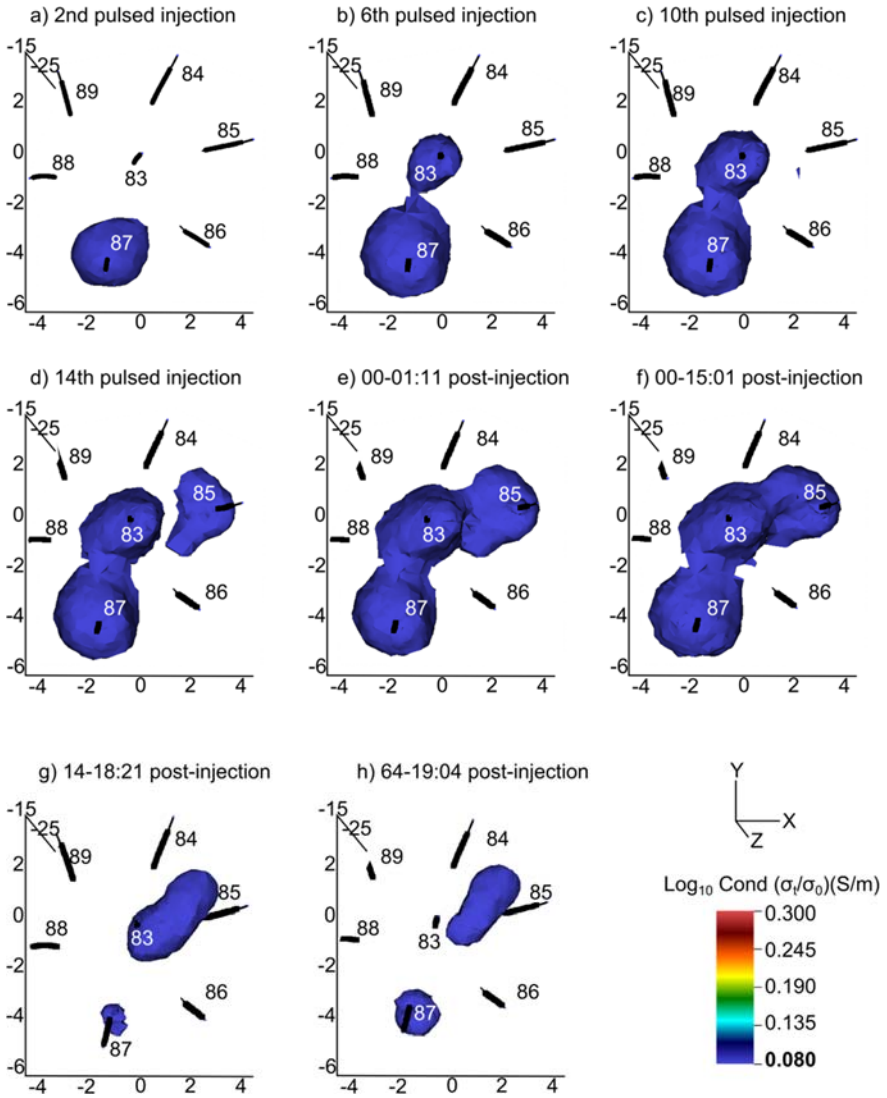

Figure 18. Plan view of time-lapse 3D ERT conductivity changes during and post amendment injection.

Individual figures a-h correspond to elevation views in Figure 5.6.13. One contour equal to 0.08 S/m is used as an image threshold.

The time-lapse ERT measurements provide valuable information at a plot scale appropriate for capturing migration pathways under a pulsed-amendment injection test. The 3D spatial extent of the tracer migration highlights flow and transport within this heterogeneous fractured rock system. Available geologic data and the hydraulic connections inferred from the drawdown data are consistent with the migration pathways imaged in Figures 17 and 18. The 3D extent of the amendment could not have been resolved using standard borehole geophysical methods or hydraulic testing alone. For example, while the ERT images generally show tracer migration pathways that are down-dip in the direction of strike, a complex, channelized flow is revealed (Figures 17e-f), particularly in the transport of the amendment around 86BR. The images of the amendment injection show strong evidence for channelized flow within the bedding plane fracture zone and provide unique temporal information on the evolution of the amendment into this zone.

6.0 PERFORMANCE ASSESSMENT

6.1 ASSESSMENT OF CHARACTERIZATION IMAGING AT NAWC

Borehole geophysical logs represent the gold standard when ground-truthing ERT models with regard to localized information within boreholes. The ERT inversion results from a cross-section slice along 87-83-85BR are shown alongside OTV logs for 85BR and 87BR (Figure 19). This section highlights structure along the planes of primary interest with regard to the tracer tests. Massive (M) and laminated (L) units have been annotated. Generally, lighter units correlate with less conductive massive units while darker units correlate with more conductive laminated units. Fracture intersection depths identified in the OTV logs mostly occur at the interface between a massive unit and laminated unit (e.g., M* in Figure 19). Most fracture zones are too small to be directly resolved in the ERT characterization imaging.

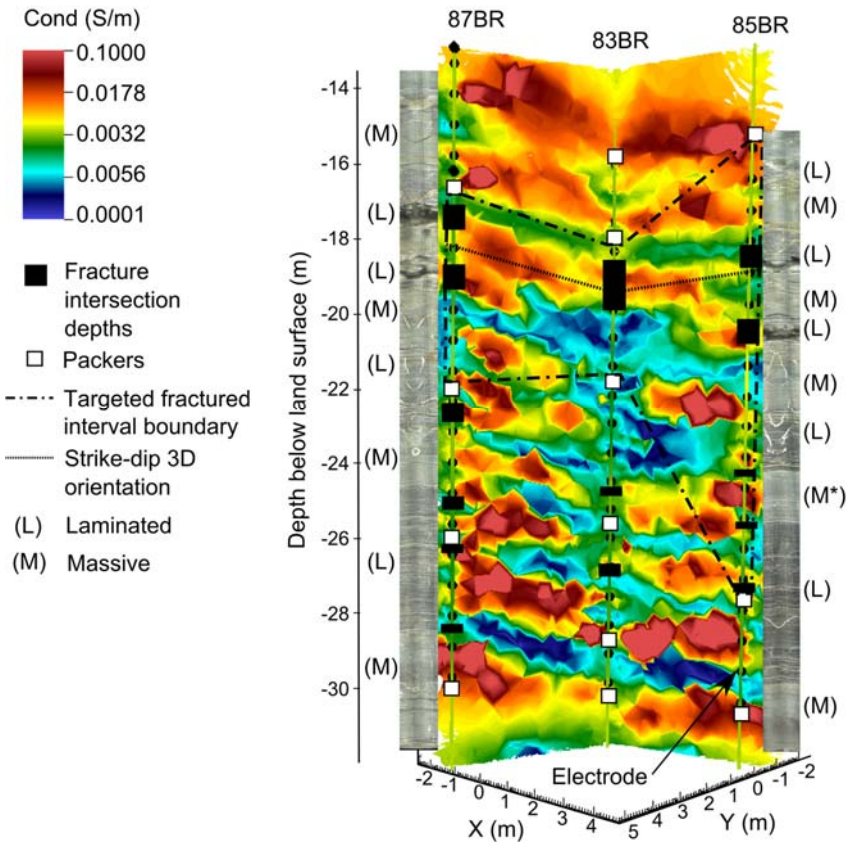

Figure 19. Electrical resistivity image for slice 85-83-87 with fracture intersection depths, packers and strike/dip of formation noted, showing alternating conductive and resistive layering partly resulting from the alternating laminated and massive mudstones at the site.
The OTV log for 85BR and 87BR is shown for comparison. In order to present an unobstructed view of 83BR, 85BR (tracer extraction well) and 87BR (tracer injection well), 86BR is not shown.

However, ERT imaging reveals an extensive electrically conductive zone between borehole pairs 87BR and 83BR, and 83BR and 85BR. This zone falls within the section defined as the targeted fractured interval boundary for the tracer injections. This was based on the highly connected (blue)

zone determined from the drawdown data acquired in the cross hole hydraulic testing (Figure 20). In summary, alternating high and low resistivity layering observed in the ERT images agree well with alternating units observed in OTV logs. The largest high conductivity feature identified in the ERT imaging coincides with the most hydraulically connected unit from hydraulic testing.

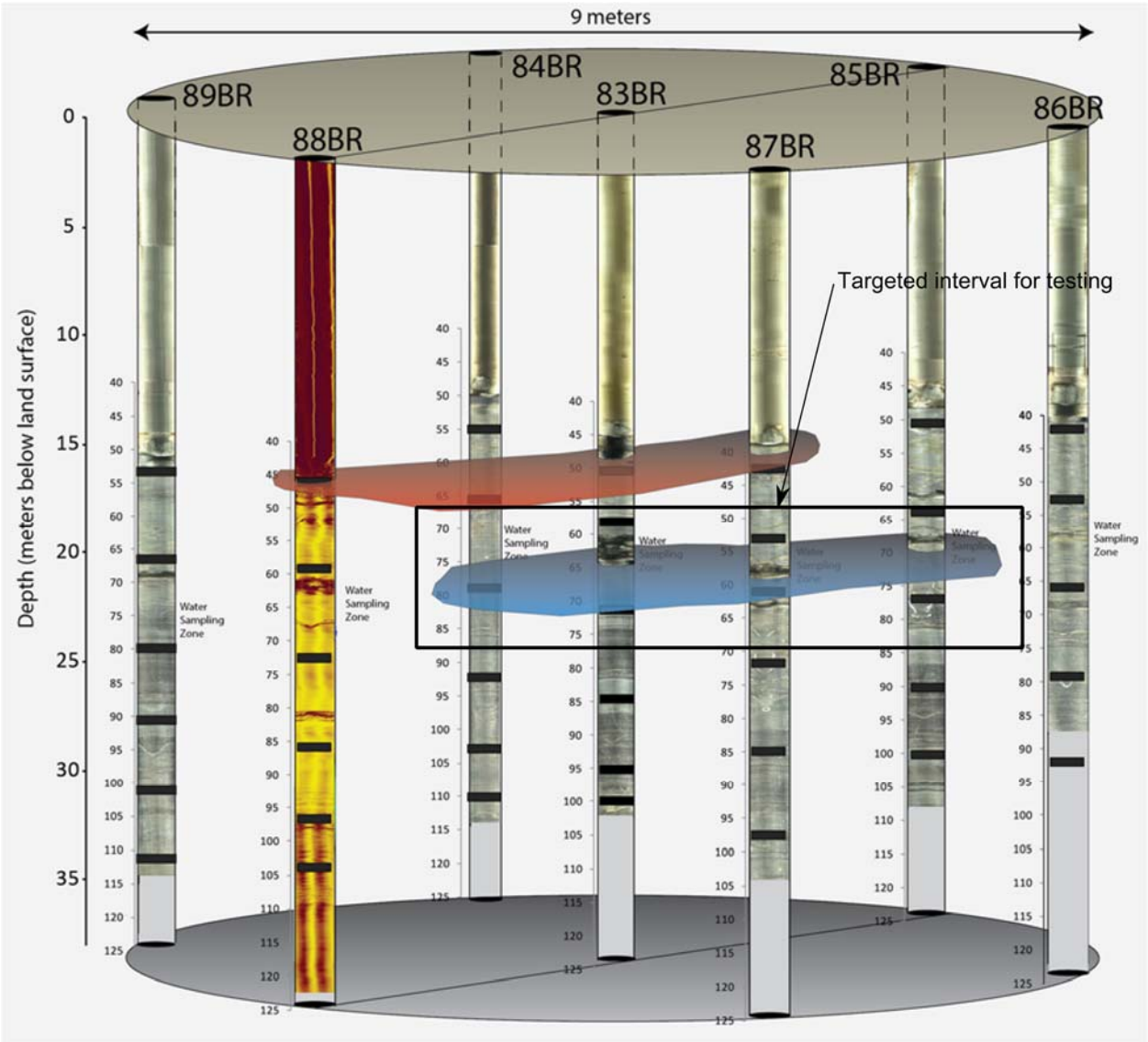

Figure 20. Interpretation of hydraulically connected pathways from cross-borehole drawdown data.

The blue zone shown between 87-83-85BR agrees well with connected units in the ERT inversion characterization model and was the targeted interval.

6.2 ASSESSMENT OF TRACER TESTS

We use the water chemistry from samples taken during each tracer and amendment test to validate overall results from ERT datasets and modeling. Note the representative element volumes (REV) of the water samples are quite different and vary by over an order of magnitude. Water samples are indicative of processes occurring at individual boreholes within the sampling zone only,

whereas ERT data can yield a comprehensive overview of changes occurring within the 83BR-89BR well field. However, ERT is only sensitive to bulk changes in conductivity, not bromide concentrations used in the tracer studies or molasses concentrations used in the amendment injections. The project team used fluid specific conductivities from localized water samples as an indicator of bulk conductivity changes likely to be detectable from ERT. Given the differences in scale and the fact that ERT data only see bulk changes in specific conductance, the project team looks to ground-truth the ERT findings with common trends in the datasets rather than absolute values.

6.2.1 87BR-85BR

Bromide and fluid specific conductance data from 85BR (only acquired during the extraction phases of the tracer test) are shown in Figure 21. After the conductive injection, there is a sharp decrease in bromide concentration and fluid specific conductance during the pulsed extraction from 85BR. This unexpected initial influx of resistive fluid into 85BR may be from radial pumping outside the circumference of the 83-89BR well field. Bromide concentrations and fluid specific conductance values subsequently increase during the continuous extraction phase after the conductive injection, indicating delayed tracer arrival. Water samples showed decreased fluid specific conductance and bromide values during the resistive injection; this was followed by increasing values (Figure 21). Between 50 and 200 hours, bromide and fluid specific conductances within 85BR decreased slightly. Extraction pumping occurred at 85BR at 200 hours, whereby a marked decrease in fluid specific conductances and bromide concentrations are shown (Figure 21). Fluid specific conductance values are well-correlated with bromide concentrations (R^2=0.67) (Figure 22a) and sulfate concentrations (R^2=0.72) (Figure 22b), but not with chloride concentrations (R^2<0.01) (data not shown for brevity).

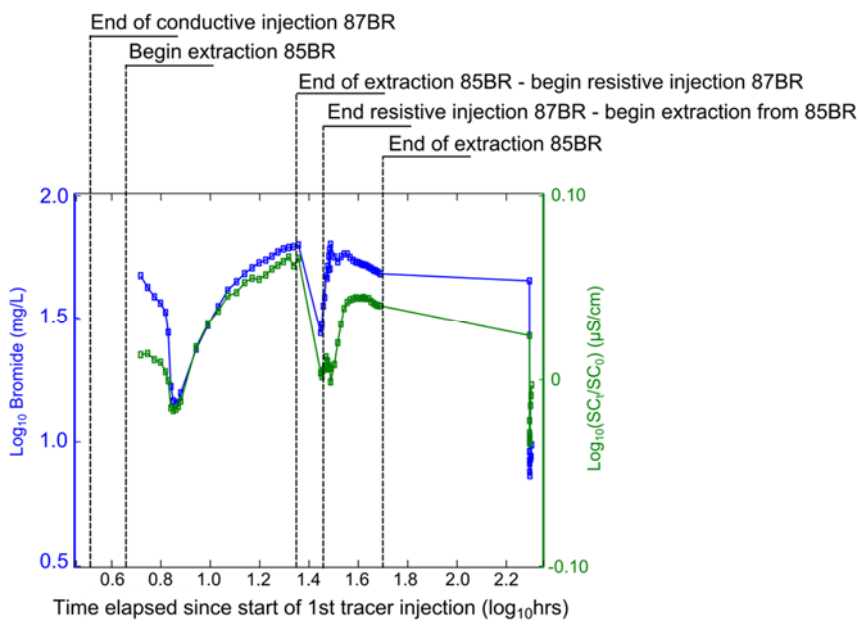

Figure 21. Fluid specific conductance and bromide concentrations for samples from 85BR during the 87BR-85BR ERT tracer injection test.

At 200 hours, 4 hours of extraction pumping at 85BR occurred.

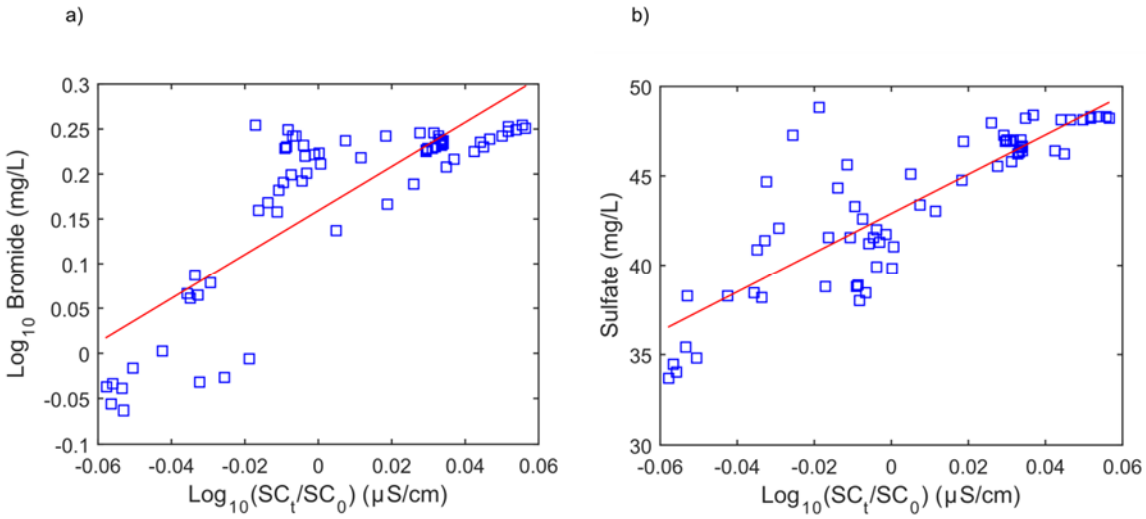

Figure 22. Bromide and changes in fluid specific conductance (SC) show similar trends in the 87-85BR tracer test (R2=0.67) (a) and sulfate concentrations and changes in SC show a significant correlation in the 87-85BR tracer test (R2=0.72) (b).

There is compelling evidence in the water sampling data that the tracers reached 85BR within the water sampling zone. However, analysis of ERT images alone might suggest that the tracer did not extend to this borehole. In this case, the sampling and analysis of water samples highlights the inherent limitations of ERT associated with image resolution even at the relatively high borehole density used in this study. Fluid specific conductance and bromide analysis of water samples from 85BR during the conductive and resistive extraction phases reveal that conductive tracer did reach 85BR (Figure 21) during the continuous extraction from this borehole although this could not be resolved in the ERT images (Figures 14-15), which only reliably show changes greater than a threshold value of 8.4%. SC readings during and following the resistive injection possibly reveal the presence of the resistive tracer at 85BR, although this again was not resolvable in the ERT images. Given the results of the hydraulic tests, tracer migration to the extraction borehole was anticipated and expected, consistent with the specific conductance and bromide analyses. ERT resolution is limited by multiple factors, including: (1) the conductivity contrast between the tracer fluid and the pore fluid in the immobile and mobile domains; (2) the possibility of narrow fracture zones important for tracer transport that are smaller than the ERT image resolution; and (3) the numerical errors in the ERT modeling that exceed the actual data errors indicated by reciprocal measurements in this case. While large conductivity contrasts between the native groundwater and the tracer fluids were used in this test (factors of 89 and ~333), dilution of the tracer caused by the subsequent extraction, combined with the relatively low conductivity contrast between the host rock and the fracture zones, probably limited the magnitude of the conductivity contrast to be less than the minimum required for ERT detection with the survey design used here. Furthermore, the ERT data may be relatively insensitive to conductivity changes within a thin fracture zone extending towards 85BR, thereby rendering the inversion unable to resolve tracer migration within the fracture.

Despite these limitations, the time-lapse ERT measurements provide valuable information at a plot scale appropriate for capturing migration pathways under a pulsed-tracer injection test. The 3D spatial extent of the tracer migration highlights flow and transport within a heterogeneous fractured

rock system. The major flow pathways observed, particularly for the conductive injection, are likely in part due to the higher-density of the bromide tracer causing down-dip migration. Available geologic data and the hydraulic connections inferred from the drawdown data are consistent with the migration pathways imaged in Figures 14-15. The 3D extent of the tracer could not have been resolved using standard borehole geophysical methods or hydraulic testing alone. For example, while the ERT images generally show tracer migration pathways that are down-dip in the direction of strike, more complexity is revealed, particularly surrounding 88BR. The images provide evidence of a convoluted tracer transport pathway extending close to 88BR and between 83BR and 87BR.

Characterizing fractured rock with ERT enhances understanding of tracer transport pathways relative to point measurements from 85BR alone. ERT imaging revealed pronounced conductivity changes occurring within 83BR, but not the extraction borehole 85BR where water samples were collected. Overall changes in ERT datasets and localized apparent conductivities within 85BR for ERT datasets agree well with water sampling trends.

6.2.2 Amendment Injection

There was limited water sampling during the amendment injection as the idea was to inject the amendment (i.e., a food supply) in pulses with no extraction well, promoting the opportunity to capture electrical signatures associated with biodegradation processes. The project team relied on the previous tracer testing between 87BR and 85BR to confirm sufficient conductivity contrast in conjunction with the pulsed injection design for the amendment injection to be imaged with ERT.

Water samples were collected prior to July 9, 2014, and 27 days after August 25, 2014, the amendment injection. The VOC analysis results are shown in Table 4 and Figure 23. Evidence of biodegradation in boreholes 83BR, 85BR and 87BR was expected since the ERT images (Section 5.6 Figures 17-18) predicted migration of the amendment near these boreholes. The project team expected to see no evidence of biodegradation in 84BR, which was predicted from hydraulic testing, borehole geophysical data, and ERT imaging.

Table 4. Water sample analysis of key compounds in boreholes 83BR, 84BR, 85BR, and 87BR prior to and after amendment injection in 87BR.

Borehole	Sample Date	TCE (µg/L)	cis-1,2-Dichloroethene (µg/L)	VC (µg/L)
83BR	7/9/2014	216.46	625.68	9.30
84BR	7/9/2014	928.11	1864.86	524.92
85BR	7/9/2014	158.50	416.46	20.74
87BR	7/9/2014	129.36	353.09	9.16
83BR	8/25/2014	56.09	596.89	13.29
84BR	8/25/2014	207.36	4096.52	504.45
85BR	8/25/2014	98.45	383.30	14.81
87BR	8/25/2014	59.44	325.26	7.32

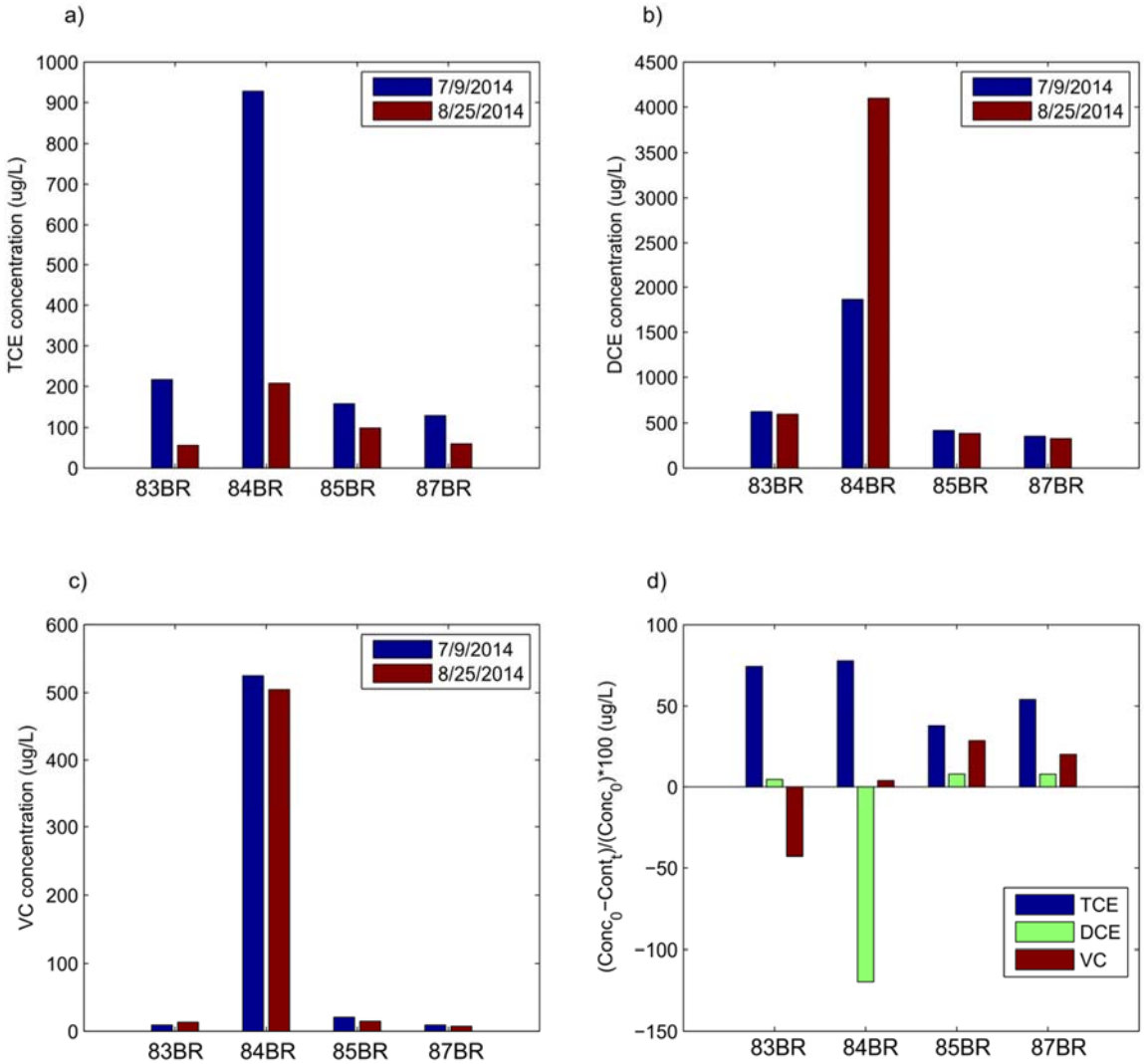

Figure 23. A visual comparison of absolute changes in a) TCE; b) DCE; c) VC concentrations prior to and after the amendment injection within sampled boreholes 83BR, 84BR, 85BR and 87BR; and d) Percent changes in concentrations from initial values (7/9/2014) of TCE, DCE and VC within 83BR, 84BR, 85BR, and 87BR.

Bacteria degrade TCE preferentially by reductive dehalogenation to cDCE. The cDCE then degrades to VC but usually at a slower pace than the TCE to cDCE degradation. There is evidence of TCE decreases in all wells (83BR, 84BR, 85BR, and 87BR) (Figure 5a). The only well sampled that shows a significant increase in cis-DCE is 84BR (Figure 23b). In all other wells, cDCE decreases or remains about the same. The causes for this may be: (a) the short time frame with respect to degradation processes (1 month); (b) the low concentration of molasses reaching the contaminated water in the fractures; or (c) the dilution of the water in the fractures with the injection water. There is little change in the concentrations of VC (Figure 23c), although percent changes appear high due to the low magnitudes of these concentrations (Figure 23d).

Initial water sampling provided no conclusive evidence of biodegradation induced by the amendment injection. A longer term of monitoring (beyond the duration of this demonstration project) would be needed to evaluate the effects of the amendment injection. The initial data suggests biodegradation in all the sampled boreholes, including 84BR. Any biodegradation at 84BR via input at 87BR is not supported by the borehole or ERT datasets. However, further water sampling over longer time scales than this project duration would need to be conducted to support this initial water sampling data.

The amendment injection is consistent with the movement of tracer during the 87-85BR tracer injection and indicates a channelized flow path in this bedding plane between boreholes 87-83-85BR. Such information could be used to estimate bedding plane fracture surface area affected by amendment injections.

This page was left blank intentionally.

7.0 COST ASSESSMENT

The costs associated with implementation of geophysical technology include both capital and operational costs. In this section, the project team focus on the specific technology developed and showcased in the work (i.e., the packer/electrode arrays for use in fractured-rock settings). Costs associated with geophysical logging can be readily obtained from commercial contractors.

These packer/electrode arrays were designed by the project team and fabricated at Rutgers University during the course of the project. Capital costs associated with materials and fabrication were recorded, as detailed below. The following cost model and calculations were based on costs associated with deployment at the NAWC site. Boreholes with similar construction and depth were assumed, and the base drilling costs on those seen at the NAWC site. Note that drilling costs can vary substantially with geographic area, rock type, and depth.

7.1 COST MODEL

Table 5 presents the cost elements based on implementation of time-lapse 3D electrical tomography at the NAWC site, focusing on use of the packer/electrode technology developed in this project. Under the project, seven wells were drilled to 130 feet depth and instrumented with packer/electrode arrays, giving a unit well cost of ~$12K. Cost reports include an array unit cost of $4.3K, including materials and labor for fabrication; hence the incremental cost of instrumenting a borehole is on the order of 36%. Cost savings are possible with volume pricing for large numbers (25+) of arrays or mass production of packer/electrode arrays.

Table 5. Cost model for implementation of time-lapse 3D electrical tomography at the NAWC site.

Cost Element	Data Tracked During the Demonstration	Costs	
Packer/electrode arrays with 25 electrodes and eight packers (unit cost)	Materials, fabrication costs, and deployment	Fabrication, labor 16 hrs	$800
		Materials[1]	$3,700
Drilling	Drilling contract for seven boreholes, 130' deep	$82,000 (total cost)	
Installation of arrays	Time in the field	Field technicians, 40 person-hrs	$2000
Servicing/repairing arrays	Time in the field	Field technicians, 40 person-hrs	$2000
Waste disposal and abandonments of wells	Standard disposal and abandonment, no cost tracking	NA	
ERT characterization or monitoring "snapshot"	• Field technician on site • Data analysis, assuming software access	Scientist, 16 hrs Field technician, 8 hrs	$1200 $400
Electrical power	No unique requirements recorded	NA	
Borehole geophysics	Standard pricing, no cost tracking	NA	
Transportation/mobilization	Standard pricing, no cost tracking	NA	
Software for ERT data analysis	Public-domain codes used in this work, otherwise standard pricing	NA	
Long-term monitoring	• Cost per 'snapshot' • Additional site visits and data analysis, with cost savings based on previous work setting up data analysis	Scientist, 4 hrs Field technician, 8 hrs	$300 $400

[1] Materials include packer core ($840), electrodes ($1,125), bladder tubing ($150), wire ($250), PVC pipe ($413), connectors ($500), and sampling tubing ($161), assuming 25 electrodes, 8 packer cores, and wells ~130 feet deep.

Costs are also reported for fieldwork and data analysis associated with baseline characterization and subsequent site visits for additional time-lapse snapshots. Note that costs are not included for transportation or mobilization. Although transportation costs were minor for the project, as the site is close to both Rutgers and the USGS NJ office, these costs are highly site- and project-dependent and must be considered for future implementations.

7.2 COST DRIVERS

The major cost driver responsible for variation in costs between different deployments centers on drilling costs. Use of the packer/electrode arrays requires boreholes, the cost of which is a function of rock type, local economics, distance between the site and drilling contractors (i.e., mobilization costs), local or state regulations for well abandonment procedures, etc. Drilling costs, however, also drive costs for conventional sampling and testing and thus are not prohibitive for geophysical work.

7.3 COST ANALYSIS

In this section, the costs associated with implementation of the technology operationally is presented along with a comparison of the technology and conventional sampling to quantify the economic value of geophysical information. Cost analysis is based on a fractured-rock site, with characteristics similar to the NAWC site (e.g., shallow water table, depth to bedrock on the order of 50 feet, and total depth of boreholes on the order of 100 feet). Drilling costs are assumed to be separate from the geophysical effort; thus, the geophysical effort is leveraging existing infrastructure. The project team assume access to electrical power on site and infrastructure for housing of instrumentation. Also assumed was a secure site, such that geophysical infrastructure is protected from vandalism and (or) theft. The goals of geophysical imaging are assumed to focus on monitoring the injection of amendments to identify the region affected by amendment. Three possible application scenarios were considered with varying goals, complexity, and cost: (1) monitoring a single amendment injection at one location, with one post-injection ERT 'snapshot;' (2) long-term monitoring at a single amendment injection location, with multiple ERT 'snapshots' collected on different occasions (Table 6); and (3) monitoring a single amendment injection at multiple locations across a site, in one post-injection field campaign. Only Scenario 2 is presented here for brevity (see the full report for details on Scenario 1 and 3). In Scenario 2, the project team envisioned a longer-term effort to track the amendment over time as it migrates from one injection location. Data collection on a quarterly basis for two years following amendment injection was assumed, producing a total of six post-injection snapshots. The total cost for scenario 2 is $43,100.

Table 6. Cost model for implementation of time-lapse 3D electrical tomography under scenario 2.

Cost Element	Description	Costs	
Seven Packer/electrode arrays (total cost)	Materials, fabrication costs, and deployment	Fabrication, labor 16 hrs	$5,600
		Materials	$25,900
Installation of arrays	Time in the field	Field technicians, 80 person-hrs	$2,000
Waste disposal and abandonments of wells	Standard disposal and abandonment, no cost tracking	NA	
ERT characterization "snapshot"	• Field technician on site • Data analysis, assuming software access	Scientist, 16 hrs Field technician, 8 hrs	$1,200 $400
Six subsequent ERT "snapshot"	• Field technician on site • Data analysis, assuming software access	Scientist, 48 hrs Field technician, 48 hrs	$3,600 $2,400
Transportation/mobilization	Travel and shipping (local assumed)		$2,000
			$43,100

Cost-benefit analysis for geophysical surveys is challenging because the information content of geophysical results includes both qualitative and quantitative aspects, and geophysical information is never a direct substitute for conventional methods, but a complement. The project team contends that the appropriate use of geophysical imaging is to fill gaps in space and (or) time between conventional samples. Based on this idea, the team seeks to quantify the economic value of geophysical results by estimating the number of conventional wells required to give the same information as a set number of geophysical wells. This analysis was performed using a hypothetical model closely based on experimental results from NAWC, collected in this project.

Using the ERT results from the amendment injection at NAWC, a realistic but hypothetical 3D electrical conductivity model was developed for amendment distribution at the site (Figure 24a). The surface area of the amendment-affected fracture zone is 40.6 m^2. In a "synthetic modeling experiment," hypothetical ERT data for this model can compute, corrupt the data with random 5% Gaussian noise, and analyze the data using the same approach as applied to real field data from NAWC, thereby obtaining the result in Figure 24b. The ERT result does not provide perfect resolution of the amendment plume, but rather provides a smooth image of reality, as is expected from geophysical imaging. Based on the ERT results, one would infer the amendment-treated area has a surface area of 28.9 m^2.

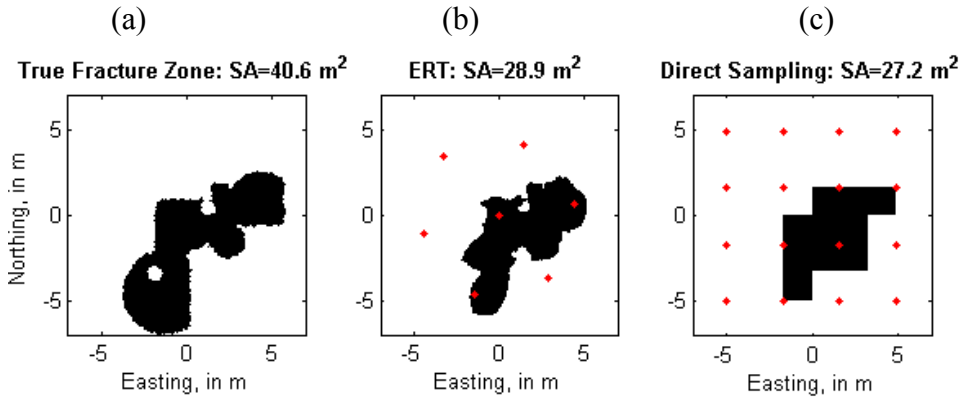

Figure 24. (a) Hypothetical amendment-treated fracture zone including surface area calculation, (b) estimated amendment-treated fracture zone based on ERT between 7 boreholes, and (c) estimated amendment-treated fracture zone inferred from direct sampling at 16 wells on a regular grid.

In the absence of geophysical imaging capabilities, one might interpolate a plume boundary based on data collected on a regular grid of wells in the same area, obtaining the result shown in Figure 24c. The conventional results for 9 or 16 wells on a regular grid provide surface-area estimates of 19.7 and 27.2, respectively. We grid spacings with 9-225 boreholes and estimate surface area for each spacing (Figure 25) was considered. This analysis shows that conventional sampling on a regular grid requires on the order of 70 wells to reliably obtain surface-area estimates equal to or superior to those obtained from 3D ERT using 7 wells. Although specific to the NAWC-site problem characteristics and fracture-zone geometry considered here, the ERT-instrumented wells could be considered to provide 10X the information content of conventional sampling on a regular grid. These results serve to underscore the value of electrode-instrumented relative to conventional wells. Assuming an incremental cost of ~36%, instrumenting wells with electrodes is highly cost effective.

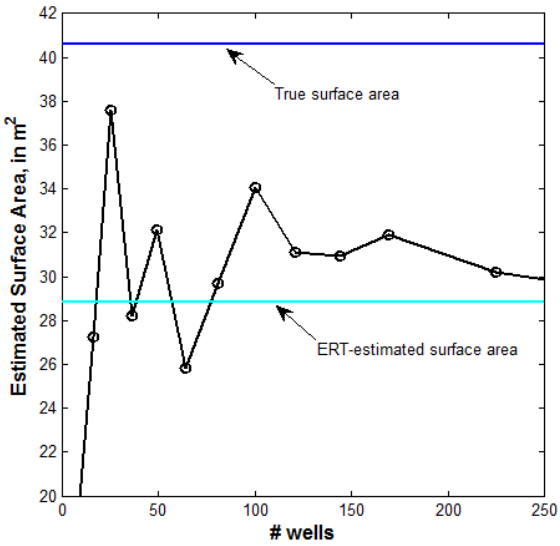

Figure 25. Estimated surface area for direct sampling on a regular grid, compared to ERT-estimated surface area for 7 wells, and true surface area.

Conventional sampling on a regular grid requires 70+ wells to reliably perform better than ERT with 70 wells.

8.0 IMPLEMENTATION ISSUES

8.1 REGULATORY ISSUES

Most of the technologies explored in the FRGT are not subject to any specific regulations beyond what is typical for working in boreholes at contaminated sites and acquiring samples (i.e., 40 hour Hazardous Waste Operations and Emergency Response [HAZWOPER] training). Unlike older neutron probes for porosity measurements, the nuclear magnetic resonance borehole tool does not involve an active neutron source, and no specific regulations apply to this tool.

Some states regulate the length of open holes to prevent cross contamination between multiple fractures or aquifers connected to the borehole. This demonstration required open hole intervals in excess of 55 feet. State of New Jersey permitting restricts open hole intervals to 25 feet. The project team requested a deviation from the state Department of Environmental Protection, and the deviation was readily obtained for this project given the nature of the site and the research program. However, such deviations may prove problematic at some sites. Regulations on open holes vary from state to state.

Metal borehole casings would prevent the effective use of most geophysical techniques included in the FRGT, although some of the tools in the FRGT can operate effectively though PVC casing. For example, borehole GPR data can be effectively acquired in PVC cased holes, and some geophysical logging tools based on the principles of electromagnetic induction can be used to obtain borehole resistivity profiles in PVC-cased holes. However, ERT and induced polarization (IP) methods used extensively in this demonstration cannot be run in PVC cased holes. The exception is when the PVC casing is slotted screen (as used in groundwater supply wells or piezometers), as the slots permit electrical contact with the formation.

Note that technology developed in the course of this research—electrode/sampling/packer arrays—help to address the open-hole regulatory implementation issue, as the team can hydraulically isolate fractures while enabling tracer experiments and electrical monitoring.

8.2 END-USER CONCERNS

From the tech transfer efforts, the primary concerns expressed by remediation professionals have largely focused on the complexity of the technology and the limited exposure of the professional community to the concepts of geophysical imaging. Decision making factors regarding whether to utilize the technology mainly evolved around cost and associated benefit with respect to achieving monitoring and remediation targets.

8.3 PROCUREMENT ISSUES

Data acquisition systems used in this project are standard commercial off-the-shelf (COTS) purchases. For example, all the ERT datasets were acquired with an Iris Sycal Pro receiver that was purchased in 2003. This instrument is still sold with only minor modifications over the last 10 years.

Procurements issues rendered some proposed components of the FRGT impractical. Most significantly, the SP monitoring and inversion was abandoned due to two factors:

1. One issue was the SP electrodes. Accurate SP measurements require the construction or purchase of high quality non-polarizing electrodes. Such electrodes are relatively straightforward to purchase or construct for surface applications. However, waterproof non-polarizing electrodes designed to work at the hydrostatic pressures associated with the investigation depths at NAWC (and other demonstration sites considered) are not readily available and challenging to construct. The project team located one vendor (Geonesis, France) but the waterproof electrodes were approximately $200 each and not guaranteed to work at the +50 feet of hydrostatic pressure at NAWC. Furthermore, the ERT deployment involved 144 electrodes and a similar array configuration for the SP monitoring was planned; the procurement cost of $29K on electrodes alone was not in the budget for the project and was not considered worth the investment given the uncertainty regarding whether the electrodes would perform at the planned depths. The team experimented with constructing waterproof SP electrodes in the laboratory but with limited success.
2. A second issue was how to incorporate the SP electrodes on the integrated packer-electrode-water sampling arrays constructed for the ERT monitoring. It was not clear how this could be done without sacrificing the effectiveness of the ERT data acquired during the project. When coupled to the uncertain value of the SP component of the FRGT (being one of the least developed methods), abandoning the SP measurements was considered the most appropriate course of action so that efforts could be focused on the other components of the FRGT that are closer to implementation by end users.

ERT data analysis codes are increasingly available through appropriate licensing agreements (commercial versus academic). This demonstration supported the development and licensing of the ERT code that was used for all the image analysis. With partial support provided from this project, co-PI Tim Johnson developed his ERT code E4D (https://e4d.pnnl.gov/Pages/Home.aspx) for public use with no licensing restriction. Commercial codes also now exist, for example ERT Lab produced by MPT Technologies (http://www.mpt3d.com/software.html). However, commercial codes may be limited in terms of the complexity of the problem (number of electrodes, number of data) they can handle. One consideration for large imaging problems as demonstrated in this project is available computing power. The large finite element models used to predict theoretical measurements based on assumed resistivity structures require large amounts of memory and processing power. For example, each 3D image of the resistivity structure at NAWC took 55 minutes to create using 144 processors on the Pacific Northwest National Laboratory (PNNL) high performance computing cluster available to this demonstration project.

In-borehole instrumentation was based on a custom-built prototype developed specifically for this demonstration. It included a novel first-of-a-kind integration of electrodes, packers for isolating sections of boreholes and water sampling ports for assessment. No COTS equivalent for this assembly currently exists. However, it is possible to purchase COTS electrode arrays for down-borehole applications (e.g., MPT Technologies offers such arrays) but these will not include any infrastructure for isolating sections of a borehole or for groundwater sampling. This currently

represents the largest procurement issue preventing end users from adapting the ERT component of the FRGT that was the focus of this specific demonstration.

9.0 REFERENCES

Ellefsen, K.J., W.C. Burton, and P.J. Lacombe, 2012. Integrated characterization of the geologic framework of a contaminated site in West Trenton, New Jersey. Journal of Applied Geophysics, 79, 71-81.

Goode, D.J., T.E. Imbrigiotta, and P.J. Lacombe, 2014. High-resolution delineation of chlorinated volatile organic compounds in a dipping, fractured mudstone: Depth- and strata-dependent spatial variability from rock-core sampling. Journal of Contaminant Hydrology. doi:10.1016/j.jconhyd.2014.10.005.

Johnson, T.C., R.J. Versteeg, F.D. Day-Lewis, W. Major, and J.W. Lane, 2014. Time-Lapse Electrical Geophysical Monitoring of Amendment-Based Biostimulation. Groundwater. doi: 10.1111/gwat.12291.

Johnson, T.C., R.J. Versteeg, A. Ward, F.D. Day-Lewis, and A. Revil, 2010. Improved hydrogeophysical characterization and monitoring through parallel modeling and inversion of time-domain resistivity and induced-polarization data. Geophysics, 75(4), WA27-WA41.

Lacombe, P.J., and W.C. Burton, 2010. Hydrogeologic Framework of Fractured Sedimentary Rock , Newark Basin , New Jersey, (2), 35–45. doi:10.1111/j1745.

Robinson, J., L. Slater, T. Johnson, A. Shapiro, C. Tiedeman, D. Ntarlagiannis, C. Johnson, F. Day-Lewis, P. Lacombe, T. Imbrigiotta, and J. Lane Jr., 2015. Imaging transport pathways in fractured rock using 3D time-lapse electrical resistivity tomography, Ground Water, DOI: 10.1111/gwat.12356. Published online 04/07/15.

Slater, L., and A. Binley, 2003. Evaluation of permeable reactive barrier (PRB) integrity using electrical imaging methods, Geophysics, 68, 3, 911-921.

Slater, L.D., F.D. Day-Lewis, D. Ntarlagiannis, M. O'Brien, and N. Yee, 2009. Geoelectrical measurement and modeling of biogeochemical breakthrough behavior during microbial activity, Geophys. Res. Lett., 36, L14402, doi:10.1029/2009GL038695.

Slater, L.D., A. Binley, and D. Brown, 1997. Electrical imaging of fractures using ground-water salinity change. Ground Water 1997, 35, (3), 436-442.

Tiedeman, C.R., P.J. Lacombe, and D.J. Goode, 2010. Multiple well-shutdown tests and site-scale flow simulation in fractured rocks. Ground Water, 48(3), 401–15. doi:10.1111/j.1745-6584.2009.00651.x.

This page was left blank intentionally.

APPENDIX A

POINTS OF CONTACT

Point of Contact	Organization	Phone Fax E-Mail	Role in Project
Lee D. Slater	Department of Earth & Environmental Sciences Rutgers-Newark 101 Warren Street, Smith 136 Newark, NJ 07102	Tel: 973-353-5109 Fax: 973-353-1965 lslater@rutgers.edu	Principal Investigator
Fred Day-Lewis	U.S. Geological Survey, Office of Groundwater, Branch of Geophysics 11 Sherman Place, Unit 5015 Storrs, CT 06269	Tel: 860-487-7402 x21 Fax: 860.487.8802 daylewis@usgs.gov	Co-Principal Investigator
Timothy Johnson	Energy and Environment Directorate Pacific Northwest National Laboratory 902 Battelle Boulevard P.O. Box 999, MSIN K9-33 Richland, WA 99352	Tel: 509-372-4715 Fax: 509-372-6089 tj@pnl.gov	Co-Principal Investigator
Allen Shapiro	U.S. Geological Survey National Research Program 12201 Sunrise Valley Drive Mail Stop 431 Reston, VA 20192 USA	Tel: 703-648-5884 Fax: 703-648-5274 ashapiro@usgs.gov	Co-Principal Investigator
John W. Lane	U.S. Geological Survey, Office of Groundwater, Branch of Geophysics 11 Sherman Place, Unit 5015 Storrs, CT 06269	Tel: 860-487-7402 x13 Fax: 860-487-8802 jwlane@usgs.gov	Co-Principal Investigator
Andrea Leeson	SERDP & ESTCP 4800 Mark Center Drive Suite 17D08 Alexandria, VA 22350	Tel: 571-372-6565 Fax: 571-372-6386 andrea.leeson.civ@mil.mail	Environmental Restoration Program Manager